Journal of Neuroinflammation

RESEARCH

Open Access

The dopamine analogue CA140 alleviates AD pathology, neuroinflammation, and rescues synaptic/cognitive functions by modulating DRD1 signaling or directly binding to Abeta

Sehyun Chae[1†], Hyun-ju Lee[2†], Ha-Eun Lee[3†], Jieun Kim[2], Yoo Joo Jeong[2,7], Yuxi Lin[4], Hye Yun Kim[3], Geoffray Leriche[5], Rachel S. Ehrlich[5], Sascha Castro Lingl[5], Min-Duk Seo[6], Young-Ho Lee[4,8,9], Jerry Yang[5*], Jae-Ick Kim[3*] and Hyang-Sook Hoe[2,7,10*]

Abstract

Background We recently reported that the dopamine (DA) analogue CA140 modulates neuroinflammatory responses in lipopolysaccharide-injected wild-type (WT) mice and in 3-month-old 5xFAD mice, a model of Alzheimer's disease (AD). However, the effects of CA140 on Aβ/tau pathology and synaptic/cognitive function and its molecular mechanisms of action are unknown.

Methods To investigate the effects of CA140 on cognitive and synaptic function and AD pathology, 3-month-old WT mice or 8-month-old (aged) 5xFAD mice were injected with vehicle (10% DMSO) or CA140 (30 mg/kg, i.p.) daily for 10, 14, or 17 days. Behavioral tests, ELISA, electrophysiology, RNA sequencing, real-time PCR, Golgi staining, immunofluorescence staining, and western blotting were conducted.

Results In aged 5xFAD mice, a model of AD pathology, CA140 treatment significantly reduced Aβ/tau fibrillation, Aβ plaque number, tau hyperphosphorylation, and neuroinflammation by inhibiting NLRP3 activation. In addition, CA140 treatment downregulated the expression of *cxcl10*, a marker of AD-associated reactive astrocytes (RAs), and *c1qa*, a marker of the interaction of RAs with disease-associated microglia (DAMs) in 5xFAD mice. CA140 treatment also suppressed the mRNA levels of *s100β* and *cxcl10*, markers of AD-associated RAs, in primary astrocytes from 5xFAD mice. In primary microglial cells from 5xFAD mice, CA140 treatment increased the mRNA levels of markers of homeostatic microglia (*cx3cr1* and *p2ry12*) and decreased the mRNA levels of a marker of proliferative region-associated microglia (*gpnmb*) and a marker of lipid-droplet-accumulating microglia (*cln3*). Importantly, CA140 treatment rescued scopolamine (SCO)-mediated deficits in long-term memory, dendritic spine number, and LTP impairment. In aged 5xFAD mice, these effects of CA140 treatment on cognitive/synaptic function and AD pathology were regulated

[†]Sehyun Chae, Hyun-ju Lee, Ha-Eun Lee contributed equally to this study.

*Correspondence:
Jerry Yang
jerryyang@ucsd.edu
Jae-Ick Kim
jikim220@unist.ac.kr
Hyang-Sook Hoe
sookhoe72@kbri.re.kr
Full list of author information is available at the end of the article

by dopamine D1 receptor (DRD1)/Elk1 signaling. In primary hippocampal neurons and WT mice, CA140 treatment promoted long-term memory and dendritic spine formation via effects on DRD1/CaMKIIα and/or ERK signaling.

Conclusions Our results indicate that CA140 improves neuronal/synaptic/cognitive function and ameliorates Aβ/tau pathology and neuroinflammation by modulating DRD1 signaling in primary hippocampal neurons, primary astrocytes/microglia, WT mice, and aged 5xFAD mice.

Keywords CA140, Dopamine D1 receptor, Learning and memory, LTP, Aβ, Tau, Reactive gliosis

Background

Extracellular senile plaque (SP) deposition and intraneuronal neurofibrillary tangle (NFT) accumulation are the predominant pathophysiological hallmarks of Alzheimer's disease (AD) [1]. SPs are aggregates of misfolded amyloid-β (Aβ), and NFTs are composed of abnormally hyperphosphorylated microtubule-associated tau proteins [1]. The accumulation of SPs and NFTs begins in the entorhinal cortex and hippocampus, brain regions associated with memory processing, and the resulting axonal deterioration, decreased dendritic spine density, neuronal loss, and weakened synaptic strength lead to cognitive dysfunction [2]. Under pathological conditions, SPs accelerate the transition of homeostatic microglia to disease-associated microglia (DAMs), neurodegenerative phenotype microglia (MGnDs), and lipid-droplet-accumulating microglia (LDAMs) and the transition of naïve astrocytes to AD-associated reactive astrocytes (RAs) [3–5]. The interaction of DAMs/MGnDs with RAs exacerbates neuroinflammatory dynamics, a key mechanism of the pathoprogression of neurodegenerative diseases, including AD. Therefore, small molecules that prevent harmful interactions of Aβ and tau with the cellular environment and SP- or NFT-mediated neuroinflammation may have therapeutic value for AD [6].

Dopamine (DA) receptors ($DRD_{1\text{-}5}$) are distributed throughout the hippocampus during hippocampal formation, and DA signaling modulates learning, memory, and dendritic spine formation [7–9]. Brain levels of DA and its receptor DRD1/DRD2 are lower in AD patients than in healthy controls, and supplementation with DA precursors or agonists rescues synaptic and cognitive function [10, 11]. In medium spiny neuronal cultures, DA promotes dendritic spine formation via DRD1 and DRD2 and participates in dendritic spine enlargement and structural plasticity [12]. Pharmacological activation of DRD1 enhances recognition memory in rats [13], and DRD1/5 activation in the rat hippocampus promotes initial and novel memory consolidation [14]. DRDs expressed on glial cells function in anti-inflammation by downregulating microgliosis and astrocytic activation; accordingly, DA regulates neuroinflammation in neurodegenerative diseases [15]. For example, the DA precursor levodopa attenuates LPS- or α-synuclein-mediated NLRP3 inflammasome activation in human microglial cultures [16]. Collectively, these observations suggest that DA and DRDs play important roles in synaptic and cognitive function and neuroinflammatory responses.

In a direct application of these findings, we recently designed and synthesized the DA analogue CA140 by introduction of a 2-(methylamino) benzoyl group to the amine in DA [17]. CA140 penetrates the blood–brain barrier (brain:plasma concentration ratio = 1.91 ± 0.22) and inhibits neuroinflammatory responses in LPS-injected wild-type (WT) mice and in 3-month-old 5xFAD mice [17]. However, the effects of CA140 on synaptic/cognitive function and AD pathology under normal and pathological conditions have not been examined. In the present study, we aimed to investigate these effects and their molecular mechanisms of action in vitro and in vivo. We found that CA140 directly bound Aβ aggregates in vitro. In aged 5xFAD mice, CA140 treatment decreased Aβ/tau fibrillation; Aβ plaque number; tau hyperphosphorylation; microgliosis/astrogliosis; and the expression of the neuroinflammation molecular target NLRP3, a marker of AD-associated reactive astrocytes (*cxcl10*), and a marker of the interaction of RAs with disease-associated microglia (DAMs; *c1qa*). In primary astrocytes (PACs) and primary microglial cells (PMCs) from 5xFAD mice, CA140 treatment suppressed the mRNA levels of markers of AD-associated RAs (*s100β* and *cxcl10*), proliferative region-associated microglia (PAMs; *gpnmb*) and lipid-droplet-accumulating microglia (LDAMs; *cln3*) and increased the mRNA levels of markers of homeostatic microglia (*cx3cr1* and *p2ry12*). More importantly, CA140 treatment attenuated memory impairment, dendritic spine loss and LTP impairment in aged 5xFAD mice by modulating DRD1/Elk1 signaling. We then investigated the effects of CA140 on synaptic/cognitive function under normal conditions and found that CA140 treatment improved synaptic and cognitive function through DRD1/CaMKIIα and/or ERK signaling in primary hippocampal neurons and WT mice. Taken together, our data indicate that the dopamine analogue CA140 modulates synaptic/cognitive function, AD pathologies, reactive gliosis, and neuroinflammatory responses through DRD1 signaling in primary hippocampal neurons, PACs, PMCs, WT mice, and aged 5xFAD mice.

Methods

Mouse studies

All in vivo experiments were performed in accordance with approved animal protocols and guidelines established by the Korea Brain Research Institute (IACUC-2016-0013, IACUC-2018-0018) and UNIST (UNISTIACUC-20-18). Male C57BL6/N mice were used as WT mice, and F1 generation 5xFAD transgenic (Tg) mice were used as the mouse model of AD.

Wild-type mice

Male C57BL6/N mice (3 months old, 25–30 g) were purchased from Orient-Bio Company (Gyeonggi-do, South Korea) and housed in a pathogen-free facility under a 12-h light/dark cycle at an ambient temperature of 22 °C. To investigate whether CA140 modulates cognitive/synaptic function and its molecular mechanisms of action under normal conditions, WT mice were injected with vehicle (10% DMSO) or CA140 (30 mg/kg, i.p.) daily for 10, 14, or 17 days. CA140 was synthesized as described previously [17], and all mice were randomly assigned to treatment groups. An independent researcher blinded to the experiments quantified all in vivo results.

5xFAD mice (mouse model of AD)

To ensure the integrity of the genetic background [18], F1 generation 5xFAD transgenic (Tg) mice (stock #34848-JAX, B6Cg-Tg APPSwFlLon, PSEN1*M146L*L286V6799Vas/Mmjax) were purchased from Jackson Laboratory. Only male mice were used to minimize bias caused by hormonal fluctuations in female AD mice. To examine the effects of CA140 on cognitive and synaptic function and AD pathologies and its molecular mechanisms of action under pathological conditions, 8-month-old 5xFAD mice were injected daily with vehicle (10% DMSO) or CA140 (30 mg/kg, i.p.) for 14 or 17 days. Behavioral experiments and tissue analysis were subsequently conducted.

Cell lines and cAMP assay

To determine whether CA140 acts as a DRD1 agonist or antagonist, we used HEK293 cells, which have high transfection efficiency for plasmid DNA [19]. HEK293 cells were maintained in Opti-MEM® (Invitrogen) with 10% fetal bovine serum (FBS, Life Technologies, Inc.) in a 5% CO_2 incubator, seeded in 12-well plates (30×10^4 cells/well), and transiently transfected with eGFP-tagged DRD1 constructs or control constructs using FuGENE® 6 (Roche). Twenty-four hours after transfection, the HEK293 cells were washed with serum-free media and treated with a DRD1 antagonist (LE300, 10 μM) or vehicle (DMSO) for 30 min. The HEK293 cells were then treated with a DRD1 agonist (A77636, 5 μM), DA (10 or 100 μM), CA140 (10, 50, or 100 μM), or vehicle (1% DMSO) for 1 h, followed by resuspension in 200 μL of 0.1 M HCl buffer and incubation for 10 min at room temperature (RT). The cell lysates were centrifuged (600×*g*) for 10 min at 4 °C to remove cellular debris. The supernatant was used to measure cAMP levels using the cAMP complete ELISA kit according to the manufacturer's recommendations (Enzo Life Sciences, Farmingdale, NY, USA).

Primary neuronal culture, transfection, and immunocytochemistry (ICC)

Primary cortical neurons (PCNs) from embryonic day (E) 16 Swiss–Webster mice were prepared as previously described [20]. In addition, primary hippocampal neurons (PHNs) from E19 Sprague–Dawley rats were cultured at 150 cells/mm^2 as previously described with minor modifications [21]. Briefly, the hippocampus was dissected from the brain, washed in dissection dissociation medium (DDM), and dissociated with trypsin. The PHNs were plated on poly-D-lysine-coated coverslips in MEM containing 10% fetal bovine serum, 1 mM pyruvate, 2 mM L-alanyl-L-glutamine dipeptide, and 0.45% glucose. Two hours after plating, the DDM was replaced with neurobasal medium supplemented with B27, Ara-C (0.5 μM), and 2 mM L-alanyl-L-glutamine dipeptide. Twice weekly, one-half of the medium was replaced with fresh maintenance medium. At DIV 13 or 20, the PHNs were transfected with GFP using Lipofectamine 2000 (Invitrogen, Carlsbad, CA, USA).

For GFP transfection, 1 μL of Lipofectamine 2000 was diluted in 25 μL of neurobasal medium and incubated at RT for 5 min. GFP plasmid DNA (2 μg) was also diluted in 25 μL of neurobasal medium and incubated at RT for 5 min. The diluted Lipofectamine 2000 and GFP DNA were then mixed and incubated at RT for 30 min in the dark. Finally, the Lipofectamine 2000/GFP DNA mixture (50 μL) was added to each well containing PHNs. Twenty-four hours after transfection, the PHNs were treated with vehicle (1% DMSO) or CA140 (1 or 5 μM) for 24 h to examine the effects of CA140 on synaptic function. The neurons were then fixed for 10 min in 4% paraformaldehyde (PFA) at RT or methanol at −20 °C, followed by immunostaining with antibodies against spinogenesis-related molecules (i.e., DRD1, synaptophysin, PSD-95, p-ERK, and p-CaMKIIα) in GDB buffer (0.1% gelatin, 0.3% Triton X-100, 16 mM sodium phosphate pH 7.4, 450 mM NaCl) overnight. The cells were then immunostained with Alexa Fluor 555- and 488-conjugated secondary antibodies for 2 h. Detailed information on the primary and secondary antibodies is provided in Table 2. Images were acquired with an LSM 510 laser scanning confocal microscope (Zeiss). Confocal z-stack

image stacks encompassing entire dendrite segments were analyzed using MetaMorph software (Universal Imaging Corporation, Downingtown, PA, USA).

Preparation of cultures of primary astrocytes and primary microglia from 5xFAD mice

To investigate the effect of CA140 on the reactive state of glial cells in an in vitro model of AD, mixed glial cultures were prepared from 5xFAD pups at postnatal days 1–2 as previously described with modifications [22, 23]. Briefly, the pups were genotyped using genomic DNA extracted from tail snips. Then, whole brains from 5xFAD pups were filtered through 70-μm nylon mesh and cultured in low-glucose DMEM with 10% FBS, 100 U/mL penicillin, and 100 μg/mL streptomycin. The mixed glial cultures were maintained in a 5% CO_2 incubator at 37 °C for 3 weeks. To obtain PACs from 5xFAD mice, 75 T flasks containing mixed glial cells were shaken at 250 rpm on a rotary shaker at RT overnight. The conditioned culture medium was then discarded, and the cells were dissociated with 0.25% trypsin–EDTA and centrifuged at 2000 rpm for 10 min. After centrifugation, the pellet (PACs) was collected and used for experiments. To isolate PMCs from 5xFAD mice, mixed glial cells were treated with mild trypsin digestion (0.5 M EDTA, 1 M $CaCl_2$, and 0.25% trypsin–EDTA in low-glucose DMEM with 1% penicillin and streptomycin) for 40 min in a 37 °C incubator. After removing the astrocyte layer, the PMCs were dissociated with trypsin–EDTA (0.25%) and centrifuged twice at 2000 rpm for 10 min. Finally, the pellet (PMCs) was collected and used for experiments.

Aβ and tau inhibition assays

Expression and purification of 2N4R tau

Escherichia coli BL21-CodonPlus (DE3) cells were transformed with a pET29b plasmid encoding human tau (2N4R isoform, 441 residues) and grown at 37 ℃ in LB medium containing kanamycin (50 mg/mL). Protein expression was induced by adding 0.5 mM isopropyl β-D-thiogalactopyranoside (IPTG) at an OD_{600} of 0.5, and the cells were further grown at 37 ℃ for 4 h. The cells were harvested by centrifugation and disrupted by sonication in lysis buffer (20 mM Tris–HCl, 500 mM NaCl, 1 mM $MgCl_2$, 5 mM DTT, 1 mM EDTA, pH 6.8). The lysate was boiled for 30 min and then centrifuged at 18,000 rpm for 50 min. The supernatant was diluted and loaded onto a cation exchange column (HiTrap SP HP, GE Healthcare Life Sciences) equilibrated with 20 mM Tris–HCl (pH 6.8) containing 50 mM NaCl, 1 mM $MgCl_2$, 2 mM DTT, 1 mM EDTA, and 0.2 mM PMSF. Tau proteins were eluted with a salt gradient (100 mM to 1 M NaCl). Further purification was performed on a HiLoad 16/600 Superdex 200 prep-grade column (GE Healthcare Life Sciences) eluted with PBS buffer. The purified tau protein was concentrated by ultrafiltration (Amicon, 10 kDa cut-off, Millipore).

Estimating the binding of CA140 to aggregated Aβ42

Aggregated Aβ was prepared from commercially available monomers (GenScript USA, Inc.) using a previously reported protocol [24]. The binding of CA140 to aggregated Aβ was measured according to a previously described assay [25]. Briefly, 300 μL of solution containing a specific concentration of CA140 in 1% DMSO in Milli-Q water was incubated with or without 30 μg of aggregated Aβ to give a final solution volume of 330 μL. The incubations were performed in duplicate and allowed to reach equilibrium overnight at RT. The next day, the solution was centrifuged for 20 min at 16,000×*g* and 4 °C. The supernatant was removed, and the pellet was resuspended in 330 μL of fresh 1% DMSO in Milli-Q water. Three 100-μL aliquots of each solution were pipetted into separate wells of a black 96-well microplate, and fluorescence was measured in a microplate reader (Molecular Devices SpectraMax i3x Multi-Mode Microplate Reader) with an excitation wavelength of 330 nm and emission of 450 nm. The observed fluorescence of CA140 in the presence of Aβ was reported as the fluorescence intensity measured after subtracting the fluorescence intensity of samples containing the same amount of CA140 but no Aβ. The averages of each run were plotted with the error bars representing the standard deviation from the mean. The data were fit to the one-site specific binding algorithm to determine K_d: $Y = B_{max} \times X/(K_d + X)$, where X is the concentration of CA140 (in μM), Y is the observed fluorescence intensity, and B_{max} is the maximal observable fluorescence upon binding of CA140 to aggregated Aβ.

Preparation of solutions of Aβ42 and tau

A stock solution of monomeric Aβ42 was prepared as previously described [26]. Briefly, lyophilized Aβ42 purchased from Peptide Institute, Inc. (Osaka, Japan) was dissolved in chilled 10 mM NaOH at ~ 200 μM and sonicated in a cold-water bath for 15 s. The peptide solution was ultracentrifuged for 1 h at 40,000 rpm and 4 °C to remove large precipitates. The concentration of Aβ42 monomers was determined by measuring the UV absorbance at 280 nm using a molar extinction coefficient of 1490 M^{-1} cm^{-1}. Buffer exchange of the stock solution of 2N4R tau against 20 mM sodium phosphate buffer (pH 7.5) was performed using PD-10 columns (GE Healthcare Life Sciences, Massachusetts, USA). The concentration of tau was determined by measuring the absorbance at 280 nm with a molar extinction coefficient of 7,575 M^{-1} cm^{-1}.

Thioflavin T (ThT) fluorescence assay

The ThT fluorescence assay was used to monitor amyloid fibrillation of Aβ42 and 2N4R tau at 37 °C. The following sample solutions were prepared: (1) 5 μM Aβ42, 20 mM sodium phosphate buffer (pH 7.5), and 5 μM ThT with and without 5, 25, 50, and 100 μM CA140; (2) 30 μM tau, 20 mM sodium phosphate buffer (pH 7.5), 1 mM TCEP, 30 μM heparin, and 5 μM ThT with and without 150 and 600 μM CA140. Each sample solution (100 μL) was pipetted in quadruplicate into wells of a low-binding 96-well plate (Corning, Kennebunk, ME, USA), and the plate was firmly sealed. The kinetic profiles of Aβ42 amyloid aggregation were monitored under quiescent conditions, while tau amyloid formation was observed under continuous shaking. ThT fluorescence intensity was recorded in a SpectraMax iD3 microplate reader (Molecular Devices LLC., San Jose, CA, USA) using excitation and emission wavelengths of 445 and 490 nm, respectively.

Behavioral tests

To assess the effects of CA140 on cognitive function under normal and pathological conditions, WT mice, a mouse model of amnesia induced by scopolamine (SCO) injection, and 5xFAD mice were treated with vehicle (10% DMSO) or CA140 (30 mg/kg, i.p.), and Y-maze and novel object recognition tests were performed. The Y-maze test evaluates short-term spatial memory. The Y-maze consisted of three arms (35 cm × 7 cm × 15 cm) at angles of 120°. To conduct the test, a mouse was placed in one arm of the maze and allowed to explore freely for 5 min. Spontaneous alternations among the arms were recorded and analyzed using a video camera connected to tracking software (Ethovision XT, Noldus, Wageningen, Netherlands), and the percentage of alternations was calculated by dividing the number of alternations by the number of alternation triads. To analyze recognition and long-term memory, the novel object recognition (NOR) test was used. The apparatus for this test consisted of an open-field box (40 cm × 40 cm × 25 cm). First, each mouse was placed in the apparatus with two identical objects for 5 min as the training phase. Twenty-four hours later, the retention testing phase was performed by placing the mouse in the same apparatus with one of the previously encountered objects and one novel object for 5 min. The locations of the two objects in the arena were counterbalanced, and between trials, odor cues were eliminated by carefully cleaning the apparatus and objects with 70% ethanol. Each trial was recorded, and the exploration time was manually quantified. Exploratory behavior was defined as pointing of the mouse's nose toward an object. The novel object preference (%) was calculated from the exploration times of the novel and familiar objects: Object preference [%] = $(T_{Novel}/[T_{Familiar} + T_{Novel}]) \times 100$.

AAV-DRD1 shRNA injection

To examine whether CA140 regulates cognitive function in a DRD1-dependent manner under normal conditions, adeno-associated viral (AAV) vectors expressing shDRD1 under the control of the U6 promoter (AAV-eGFP-U6-mDRD1a-shRNA, 1.0×10^{12} genome copies [GC]/mL) and control AAV expressing GFP (AAV-eGFP-U6-shRNA) were purchased from Vector Biolabs (Malvern, PA, USA). Male WT mice (3 months old, 25–30 g) were anesthetized with 2,2,2-tribromoethanol (Sigma Aldrich, St. Louis, MO, USA, 2.5% v/v, 150 mg/kg, i.p.) and placed in a stereotaxic apparatus (Stoelting, Wood Dale, Illinois, USA). Next, the AAVs were injected bilaterally into the hippocampal CA1 region in a volume of 0.5 μL at a flow rate of 0.1 μL/min using a 10-μL Hamilton syringe and 26 G needle. The stereotaxic coordinates of the hippocampal CA1 injection site were −1.7 mm anterior/posterior (AP), ± 1.4 mm medial/lateral (ML), and −1.5 mm dorsal/ventral (DV) from the bregma. The surgery was performed 7 days before beginning the treatment regimen of daily administration of CA140 (30 mg/kg, i.p.) or vehicle (10% DMSO) for 14 days. The behavioral tests were conducted on days 15 to 17 after beginning the treatment regimen.

To examine whether CA140 regulates cognitive function in a DRD1-dependent manner under pathological conditions, 8-month-old 5xFAD mice were injected with AAV-eGFP-U6-shRNA or AAV-eGFP-U6-mDRD1a-shRNA in the bilateral hippocampal CA1 region in a volume of 1.0 μL at a flow rate of 0.3 μL/min. The coordinates were −2.0 mm (AP), ± 1.5 mm (ML), and −1.55 mm (DV) from the bregma. The surgery was performed 21 days before beginning the treatment regimen of daily administration of CA140 (30 mg/kg, i.p.) or vehicle (10% DMSO) for 14 days. Behavioral tests were performed on days 15 to 17 after beginning the treatment regimen.

Golgi staining and morphological analysis of dendritic spines

To evaluate the effects of CA140 on dendritic spine formation in vivo, we conducted Golgi staining using an FD Rapid GolgiStain Kit (FD Neurotechnologies, Ellicott City, MD, USA) as described previously [27–29]. Briefly, vehicle- or CA140-injected WT and 5xFAD mice were submerged in Solutions A and B for 2 weeks in the dark and then transferred to Solution C for 24 h. Solution C was replaced after the first 24 h. Individual mouse brains were sliced at a thickness of 150 μm using a VT1000S Vibratome (Leica, Bannockburn, IL, USA). Dendritic images were acquired with an Axioplan 2 (Zeiss, Oberkochen, Germany) under brightfield microscopy. Dendritic spine density was determined by measuring

pyramidal neurons in the cortex and/or hippocampal CA1 region from −1.70 mm to −2.30 mm relative to the bregma using ImageJ (version 1.53a, National Institutes of Health, Bethesda, MD, USA).

mRNA sequencing

To investigate the molecular mechanisms (including gene profiling) by which CA140 inhibits neuroinflammatory responses in an AD mouse model, 3-month-old 5xFAD mice were injected with vehicle (10% DMSO) or CA140 (30 mg/kg, i.p.) daily for 14 days. Total RNA was then extracted from the mouse hippocampus. The integrity of the total RNA was analyzed using an Agilent Technologies 2100 Bioanalyzer. The RNA integrity number (RIN) values were > 8.8 for all samples. Poly(A) mRNA isolation from total RNA and subsequent fragmentation were performed using the Illumina TruSeq Stranded mRNA LT Sample Prep Kit according to the manufacturer's instructions. The adapter-ligated libraries were sequenced using an Illumina NovaSeq 6000 (Macrogen, Korea). mRNA-sequencing was performed for two independent replicates under each condition. Adapter sequences (TruSeq universal and indexed adapters) were removed from the resulting read sequences for each sample using cutadapt software (version 2.7; https://cutadapt.readthedocs.io/en/stable/). The remaining reads were then aligned to the *Mus musculus* reference genome (GRCm38) using TopHat2 software (version 2.1.1) with default parameters [30]. After alignment, we counted the numbers of reads mapped to the gene features (GTF file of GRCm38.91) using HTSeq [31]. Read counts for the samples in each condition were then normalized using TMM (trimmed mean of M-values) normalization in the edgeR package [32].

Identification of differentially expressed genes (DEGs)

Differential expression analysis was performed using the Bioconductor package DESeq2 (version 1.38) with default parameters [33]. DEGs were identified by adjusted p values < 0.05 and absolute $\log_2$-fold changes > 0.58 (1.5-fold change). Gene set enrichment analysis of the DEGs was performed using DAVID software [34]. Gene Ontology biological processes (GOBPs) with p values < 0.05 were selected as the processes enriched in DEGs. Cytoscape software was used to reconstruct a network model in which the nodes were arranged based on the locations and associations of the corresponding genes in the KEGG pathway and WikiPathways databases [35, 36].

Real-time quantitative PCR (qPCR)

To validate the results of mRNA sequencing, the same mRNA sample used for mRNA sequencing was reverse transcribed to cDNA using the Superscript cDNA Premix Kit II with oligo (dT) primers (GeNetBio, Chungman, Korea). In addition, to investigate the effects of CA140 on the reactive state of glial cells in AD, mRNA from CA140-treated PACs and PMCs (from 5xFAD mice) was reverse transcribed to cDNA using the Superscript cDNA Premix Kit II with oligo (dT) primers (GeNetBio, Chungman, Korea). The synthesized cDNA was then used as the template in real-time qPCR with Fast SYBR Green Master Mix (Thermo Fisher Scientific, Waltham, MA, USA) in a QuantStudio 5 Real-Time PCR System (Applied Biosystems, Thermo Fisher Scientific, Waltham, MA, USA). The primer sequences for real-time qPCR are given in Table 1. Cycle threshold (Ct) values were normalized to the value for *gapdh*, and the fold change was calculated relative to the control.

Electrophysiology

Long-term potentiation (LTP)/basal synaptic transmission

To determine the effects of CA140 on SCO-mediated suppression of LTP and basal synaptic transmission, WT mice were injected (i.p.) daily with CA140 (30 mg/kg, i.p.) or vehicle (10% DMSO) for 14 days and injected with SCO (1 mg/kg) or PBS daily on days 3 through 14. In addition, to examine the effects of CA140 on hippocampal synaptic plasticity in an aged AD mouse model, 8-month-old 5xFAD mice were injected daily with CA140 (30 mg/kg, i.p.) or vehicle (10% DMSO, i.p.) for 14 days. Acute hippocampal slices (300 μm) were obtained using a vibratome (VT1200S, Leica). The brain slices were allowed to recover for 20 min at 34 °C and 40 min at RT in artificial cerebrospinal fluid (ACSF) containing 125 mM NaCl, 2.5 mM KCl, 1.25 mM NaH_2PO_4, 25 mM $NaHCO_3$, 1 mM $MgCl_2$, 2 mM $CaCl_2$ and 15 mM glucose oxygenated with 95% O_2 and 5% CO_2. After recovery, the brain slices were transferred to a submerged recording chamber perfused with ACSF at a rate of 2–3 mL/min at 30–31 °C.

To measure basal synaptic transmission, borosilicate glass pipettes (2.5–4.0 MΩ) were filled with Cs^+-based low Cl^- internal solution containing 135 mM $CsMeSO_3$, 10 mM HEPES, 1 mM EGTA, 3.3 mM QX-314 chloride, 0.1 mM $CaCl_2$, 4 mM Mg-ATP, 0.3 mM Na_3-GTP, and 8 mM Na_2-phosphocreatine (adjusted to pH 7.3 with CsOH). For theta-burst stimulation (TBS) LTP, the glass pipettes were filled with K^+-based internal solution containing 135 mM $KMeSO_3$, 3 mM KCl, 10 mM HEPES, 1 mM EGTA, 0.1 mM $CaCl_2$, 8 mM Na_2-phosphocreatine, 4 mM Mg-ATP, and 0.3 mM Na_3-GTP (adjusted to pH 7.3 with KOH). The access resistance was 10–20 MΩ, and only neurons with a change in access resistance < 20% were included in the analysis. Pyramidal neurons in CA1 were voltage-clamped at −70 mV, and the Schaffer collateral (SC) pathway was stimulated every 20 s. Three

Table 1 Primers used in real-time qPCR

Gene		Sequence
nlrp3	Forward	5′-TCC ACA ATT CTG ACC CAC AA-3′
	Reverse	5′-ACC TCA CAG AGG GTC ACC AC-3′
il-1β	Forward	5′-TTG ACG GAC CCC AAA AGA TG-3′
	Reverse	5′-AGG ACA GCC CAG GTC AAA G -3′
iba-1	Forward	5′-GGA CAG ACT GCC AGC CTA AG-3′
	Reverse	5′-GAC GGC AGA TCC TCA TCA TT-3′
gfap	Forward	5′-GTT TCA TCT TGG AGC TTC TGC-3′
	Reverse	5′-GGA GGT GGA GAG GGA CAA C-3′
s100β	Forward	5′-TGG TTG CCC TCA TTG ATG TCT-3′
	Reverse	5′-CTC GTT GTT GAT AAG CTC CTT CAG-3′
wwtr1	Forward	5′-GTG AAG GCT TCT CGG TTG AG-3′
	Reverse	5′-ACG TCT TGC TTG CCT TGT CT-3′
neat1	Forward	5′-TGG AGA TTG AAG GCG CAA GT-3′
	Reverse	5′-ACC ACA GAA GAG GAA GCA CG-3′
cxcl10	Forward	5′-GCC GTC ATT TTC TGC CTC A-3′
	Reverse	5′-GCT TCC CTA TGG CCC TCA TT-3′
chi3l1	Forward	5′-CAA GGA ACT GAA TGC GGA AT-3′
	Reverse	5′-CTG TGA TGG CCT GTG ATT TG-3′
serpina3n	Forward	5′-CCC TGA GGA AGT GGA AGA AT-3′
	Reverse	5′-CCT GAT GCC CAG CTT TGA AA-3′
nestin	Forward	5′-AGG AGA AGC AGG GTC TAC AGA G-3′
	Reverse	5′-AGT TCT CAG CCT CCA GCA GAG T-3′
synemin	Forward	5′-GCC TTT GGA GGG TTA AGG AC-3′
	Reverse	5′-CTT AGA TAC CCC TGC CAC CA-3′
dst	Forward	5′-GCT CCC TGC TCA GAA AAC AC-3′
	Reverse	5′-CTG TGA ACG TGT GGA TGG TC-3′
tspo	Forward	5′-GCT GTG GAT CTT TCC AGA ACA-3′
	Reverse	5′-ATG CCA AGA GGG TTT CTG C-3′
mao-b	Forward	5′-GGC TGC TAC ACA ACC TAC TTC C-3′
	Reverse	5′-CAG TGT GAG GCT GTT TCA GTG-3′
hspb1	Forward	5′-GCT CAC AGT GAA GAC CAA GG-3′
	Reverse	5′-GAA GCA CCG AGA GAT GTA GC-3′
cryab	Forward	5′-AGG TGT TGG GAG ATG TGA TTG A-3′
	Reverse	5′-GGA TGA AGT AAT GGT GAG AGG GT-3′
fabp7	Forward	5′-CAA GAA CAC AGA GAT CAA TTT CCA-3′
	Reverse	5′-CAT CCA ACC GAA CCA CAG A-3′
cr3	Forward	5′-GCA GGA GTC GTA TGT GAG G-3′
	Reverse	5′-TTA CTG AGG TGG GGC GTC T-3′
c1qa	Forward	5′-AAA GGC AAT CCA GGC AAT ATC A -3′
	Reverse	5′-TGG TTC TGG TAT GGA CTC TCC-3′
cx3cr1	Forward	5′-ATT CTT CAT CAC CGT CAT CAG-3′
	Reverse	5′-ACT AAT GGT GAC ACC GTG CT-3′
p2ry12	Forward	5′-GCT GCC TTG CTG AAG TCT CT-3′
	Reverse	5′-AGG TGG TAT TGG CTG AGG TG-3′
cd164	Forward	5′-GGT TTC AGT TCC CAT GTG CT-3′
	Reverse	5′-CAA ATG AAA GCC CCA CAA CT-3′
cln3	Forward	5′-AAA CCA GAG CCA TGT GGA AC-3′
	Reverse	5′-GCT CCC AGC AGA ACA AAC TC-3′
npc2	Forward	5′-CCT GAA TAA GCT TCC GGT GA-3′
	Reverse	5′-AGT TTC CAT TCC ACC ACC AG-3′
slc33a1	Forward	5′-GAA AAC GTG GGC TAT GCT TC-3′
	Reverse	5′-CCT TCT TCC ACC AGC TTC AG-3′
snx17	Forward	5′-CTT CGA ACC TCA CTG GAA GC-3′
	Reverse	5′-CAG GGG TCA AAG AGA ACA GC-3′
gpnmb	Forward	5′-CCA ATT ACG TGG CTG GTC TT-3′
	Reverse	5′-CCC AAA TCA TTC CTG CAG TT-3′
igf1	Forward	5′-CAC AAA CTC ACC ACC CTG TG-3′
	Reverse	5′-CTC CTG GAA ACC CAG AAC AA-3′
itgax	Forward	5′- CCA AGA CAT CGT GTT CCT GAT T-3′
	Reverse	5′-ACA GCT TTA ACA AAG TCC AGC A-3′
clec7a	Forward	5′-AGA CAC AGG GAG AAG GCA AA-3′
	Reverse	5′-CAG AAA AGG TGG GCA GAC TC-3′
lpl	Forward	5′-GGG AGT TTG GCT CCA GAG TTT-3′
	Reverse	5′-TGT GTC TTC AGG GGT CCT TAG-3′
ctsd	Forward	5′-GCT TCC GGT CTT TGA CAA CCT-3′
	Reverse	5′-CAC CAA GCA TTA GTT CTC CTC C-3′
cd44	Forward	5′-ACT AGA TCC CTC CGT TTC ATC C-3′
	Reverse	5′-GGT TAC ATT CAA ATC GAT CTG CTG-3′
apoE	Forward	5′-GGT TCG AGC CAA TAG TGG AA-3′
	Reverse	5′-TAT TAA GCA AGG GCC ACC AG-3′
spp1	Forward	5′-AGC AAG AAA CTC TTC CAA GCA A-3′
	Reverse	5′-GTG AGA TTC GTC AGA TTC ATC CG-3′
trem2	Forward	5′-CAG TTT CTC CTG CTG CTG AT-3′
	Reverse	5′-CAG TGC TTC AAG GCG TCA TA-3′
grn	Forward	5′-CTG TAG TGC AGA TGG GAA ATC CTG CT -3′
	Reverse	5′-GTG GCA GAG TCA GGA CAT TCA AAC T-3′
gapdh	Forward	5′-TGT GTC CGT CGT GGA TCT GA-3′
	Reverse	5′-CCT GCTTCA CCA CCT TCT TGA -3′

successive excitatory postsynaptic currents (EPSCs) were averaged and expressed relative to the normalized baseline. TBS consisted of a burst of five pulses at 100 Hz repeated 10 times at 5 Hz. Four consecutive trains of TBS were delivered at 10-s inter-train intervals. TBS was delivered in current clamp mode. Recording signals were filtered at 2 kHz (Multiclamp 700B, Molecular Devices) and digitized at 10 kHz (NI PCIe-6259, National Instruments). Recording data were acquired online using the WinWCP program (Strathclyde software, http://spider.science.strath.ac.uk/sipbs/software_ses.htm) and analyzed offline using Clampfit 10.7 software (Molecular Devices) and OriginPro 2017 (OriginLab).

Miniature excitatory postsynaptic currents (mEPSCs)

To determine the effects of CA140 on mEPSCs in an AD mouse model, 6-month-old 5xFAD mice were injected with CA140 (30 mg/kg, i.p.) or vehicle (10% DMSO) daily for 14 days and sacrificed on the last day

of injection. To measure mEPSCs, borosilicate glass pipettes (2.5–4.0 MΩ) were filled with Cs^+-based low Cl^- internal solution containing 135 mM $CsMeSO_3$, 10 mM HEPES, 1 mM EGTA, 3.3 mM QX-314 chloride, 0.1 mM $CaCl_2$, 4 mM Mg-ATP, 0.3 mM Na_3-GTP, and 8 mM Na_2-phosphocreatine (adjusted to pH 7.3 with CsOH). Pyramidal neurons in CA1 were voltage-clamped at −70 mV to measure mEPSCs. ACSF containing 500 nM tetrodotoxin and 25 μM D-AP5 was perfused during the recording. The amplitude and frequency of the mEPSCs were analyzed with MiniAnalysis (Synaptosoft).

Immunofluorescence staining (IF)

To evaluate the effects of CA140 on AD pathology, neuroinflammation, and synaptic function under pathological conditions, 8-month-old 5xFAD mice were injected with CA140 (30 mg/kg, i.p.) or vehicle (10% DMSO) daily for 14 days. In addition, to examine whether CA140 modulates AD pathology and neuroinflammation in a DRD1-dependent manner, 8-month-old 5xFAD mice were injected with AAV-DRD1 shRNA or AAV-control shRNA in the bilateral hippocampal CA1 region. Three weeks after AAV injection, the mice were injected with vehicle (10% DMSO) or CA140 (30 mg/kg, i.p.) daily for 17 days. To assess the mechanism by which CA140 regulates cognitive/synaptic function under normal conditions, 3-month-old WT mice were injected with vehicle (10% DMSO) or CA140 (30 mg/kg, i.p.) daily for 14 days. The treated mice were perfused/fixed in 4% paraformaldehyde overnight and then in 30% sucrose solution for 2 days. A cryostat (Leica CM1850, Wetzlar, Germany) was used to obtain coronal slices with a thickness of 35 μm, which were then permeabilized at RT for 1 h in PBS containing 0.2% Triton X-100 (PBST) and 10% normal goat serum. The brain sections were immunostained for 24–72 h at 4 °C with anti-$A\beta_{17\text{-}24}$ (4G8), anti-$Tau^{Thr212/Ser214}$ (AT100), anti-Iba-1, anti-GFAP, anti-NLRP3, anti-IL-1β, anti-CXCL10, anti-C1QA, anti-GPB2, anti-CD68, anti-CD206, anti-synaptophysin, anti-PSD-95, or anti-DRD1 antibodies diluted in PBST. After incubation with the primary antibody, the sections were washed with PBST three times and incubated with the secondary antibody at RT for 2 h. Finally, the sections were washed three times with PBS and mounted in antifade mounting medium with DAPI (Vector Laboratories, Burlingame, CA, USA). Images of the sections were acquired by fluorescence microscopy (DMi8, Leica Microsystems, Wetzlar, Germany) and analyzed by the software ImageJ (version 1.53a, National Institutes of Health, Bethesda, MD, USA). Detailed information regarding the primary and secondary antibodies is provided in Table 2.

Enzyme-linked immunosorbent assay (ELISA) for plasma IL-1β and COX-2

To determine whether long-term CA140 treatment induces peripheral inflammatory responses (adverse effects), plasma IL-1β and COX-2 levels were measured by ELISA. For this experiment, WT mice were injected with water (control for vehicle), 10% DMSO (vehicle), or CA140 (30 mg/kg, i.p.) daily for 17 days, and retro-orbital blood was collected via a capillary tube. The blood was centrifuged at 2000 rpm for 10 min at 4 °C, and the plasma was collected and stored at − 80 °C until analysis. IL-1β and COX-2 levels (100 μL of plasma) were measured using IL-1β and COX-2 ELISA kits (IL-1β ELISA kit: 88-7013-88, Invitrogen, Waltham, Massachusetts, USA; COX-2 ELISA kit: DYC4198, R&D Systems, Minneapolis, MN, USA) according to the manufacturer's instructions and as previously described [28].

Western blot

To demonstrate the mechanism by which CA140 modulates synaptic and cognitive function under normal and pathological conditions, WT and 5xFAD mice were injected with vehicle (10% DMSO, i.p.) or CA140 (30 mg/kg, i.p.) daily for 17 days, and the hippocampus and/or cortex was dissected. In addition, to investigate the in vivo toxicity of CA140, the livers and kidneys of CA140-treated WT mice were collected. The brain, liver, and kidney tissues were homogenized in RIPA lysis buffer (Merck Millipore, Billerica, MA, USA) containing 1% protease and phosphatase inhibitor cocktail (Thermo Scientific, Waltham, MA, USA) for 1 h on ice. The lysates were then centrifuged twice for 15 min at 20,000×*g* and 4 °C, and the supernatant was stored at − 80 °C until analysis. To separate brain proteins by electrophoresis, 20 μg of protein was heated for 10 min at 100 °C and loaded onto an 8% SDS–polyacrylamide gel. To separate liver or kidney proteins by electrophoresis, 50 μg of protein was heated for 10 min at 100 °C and loaded onto a 10% SDS–polyacrylamide gel. The separated proteins were then electrotransferred to a PVDF membrane (Millipore, Bedford, MA, USA), which was blocked with 5% skim milk in TBST and incubated overnight with anti-pCaMKIIα, anti-pERK, anti-pELK-1, anti-caspase-3, anti-cleaved caspase-3, or β-actin antibodies at 4 °C. Next, the membrane was incubated with the horseradish peroxidase-conjugated secondary antibody for 1 h at RT. Finally, ECL solution (ATTO, Tokyo, Japan) was added for detection, and images were acquired and analyzed with the software Fusion Capt Advance (Vilber Lourmat, Eberhardzell, Germany).

Table 2 Antibodies used in IF, ICC and WB

Primary antibodies					
Immunogen	**Host species**	**Dilution**	**Manufacturer**	**Catalog no**	**Application**
4G8	Mouse	1:500	BioLegend	800,704	IF
AT100	Mouse	1:200	Invitrogen	MN1060	IF
Iba-1	Rabbit	1:500	Wako	019-19741	IF
GFAP	Chicken	1:500	Millipore	AB5541	IF
NLRP3	Goat	1:100	Abcam	AB4207	IF
IL-1β	Rabbit	1:100	Abcam	AB9722	IF
CXCL10	Goat	1:50	R&D	AF-466-NA	IF
C1QA	Rat	1:20	Abcam	AB11861	IF
GBP2	Rabbit	1:100	Abcam	AB203238	IF
CD68	Rat	1:100	Biorad	MCA1957GA	IF
CD206	Rat	1:100	Thermo	12-2061-82	IF
Synaptophysin	Rabbit	1:200	Invitrogen	MA5-14532	IF
Synaptophysin	Mouse	1:200	Sigma-Aldrich	S5768	ICC
PSD-95	Mouse	1:200	Neuromab	75028	IF, ICC
DRD1	Rat	1:200	Sigma Aldrich	D2944	IF
DRD1	Rabbit	1:200	Invitrogen	AB20066	ICC
pCaMKIIα	Rabbit	1:200	Cell Signaling	12716	WB
pCaMKIIα	Rabbit	1:200	Abcam	AB5683	ICC
pERK	Rabbit	1:2000	Cell Signaling	9101	WB
pERK	Rabbit	1:200	Invitrogen	368800	ICC
p-ELK-1^{Ser383}	Mouse	1:1000	Cell Signaling	9186	WB
GFP	Mouse	1:200	Novus	NB600-597	ICC
GFP	Rabbit	1:200	Invitrogen	A11122	ICC
Caspase-3	Rabbit	1:500	Abcam	AB32351	WB
C. caspase-3	Rabbit	1:1000	Cell Signaling	9664	WB
β-actin	Mouse	1:2000	Santa Cruz	SC-47778	WB

Secondary antibodies				
Antibody	**Dilution**	**Manufacturer**	**Catalog no**	**Application**
Goat anti-rabbit IgG, 555	1:200	Invitrogen	A21428	IF, ICC
Goat anti-mouse IgG, 555	1:200	Invitrogen	A21422	IF, ICC
Goat anti-mouse IgG, 488	1:200	Invitrogen	A11001	IF, ICC
Donkey anti-goat, 555	1:200	Invitrogen	A21432	IF
Goat anti-chicken IgG, 488	1:200	Abcam	A150169	IF
Goat anti-rat IgG, 555	1:200	Invitrogen	A21434	IF, ICC
Goat anti-rabbit, HRP	1:5000	Enzo	ADI-SAB-300-J	WB
Goat anti-mouse, HRP	1:5000	Enzo	ADI-SAB-100-J	WB

Statistical analysis

Comparisons between two groups were performed using unpaired two-tailed t-tests, whereas one-way ANOVA or two-way repeated-measures ANOVA was used for multiple comparisons. Tukey's or Dunn's multiple-comparison test was used for post hoc analyses with significance at $^{*}p < 0.05$, $^{**}p < 0.01$, and $^{***}p < 0.001$. All analyses were performed in GraphPad Prism 7 software. Data are presented as the mean ± S.E.M. Details of the statistical analyses are provided in Table S1.

Results

CA140 binds to aggregated Aβ and reduces Aβ/tau amyloid formation and Aβ/tau pathology

Several studies have demonstrated that DA interacts with aggregated Aβ and modulates Aβ metabolism [37]. Thus, we examined whether the DA analogue CA140 binds to aggregated Aβ and found that CA140 interacted with aggregated Aβ with a K_d of 7.8 ± 2.4 μM (Fig. 1A).

We investigated the influence of CA140 on $Aβ_{42}$ amyloid formation by performing ThT fluorescence assays. In the absence of CA140, the fluorescence intensity increased after a lag time of ~0.8 h and plateaued at ~2 h (Fig. 1B, C). In the presence of CA140, similar sigmoidal ThT kinetics were observed, and the intensity of ThT intensity at the saturation phase decreased with increasing CA140 concentration (Fig. 1B, C). We quantified amyloid fibrils using the ThT fluorescence intensity at the endpoint of the experiments (i.e., the final ThT intensities at 3 h) and found that as the concentration of CA140 increased from 0 to 100 μM (5 molar equivalents of CA140 with respect to the concentration of $Aβ_{42}$), the final ThT intensity decreased from ~1.6×10^6 (0 μM CA140) to ~1.3×10^6 (25 μM CA140) to ~1.0×10^6 (100 μM CA140) (Fig. 1C). These results confirmed that CA140 inhibits nucleation-limited $Aβ_{42}$ amyloid fibrillation in a dose-dependent manner.

To examine whether CA140 affects Aβ levels in vitro, primary cortical neurons (PCNs) and APP-overexpressing CHO cells were treated with vehicle (1% DMSO) or CA140 (1 or 5 μM) for 24 h, and Aβ levels were measured by ELISA. Compared with vehicle, 5 μM CA140 significantly reduced mouse and human Aβ levels in PCNs and APP-overexpressing CHO cells, respectively (Fig. 1D, E).

Next, to determine the effects of CA140 on Aβ plaque levels in aged 5xFAD mice, 8-month-old 5xFAD mice (late-phase AD mouse model with severe Aβ accumulation) were injected with CA140 (30 mg/kg, i.p.) or vehicle (10% DMSO) daily for 14 days, and brain sections were immunostained with an anti-$Aβ_{17-24}$ (4G8) antibody recognizing Aβ plaques. We found that CA140 treatment significantly reduced the number of Aβ plaques in the cortex and hippocampal DG region (but not the hippocampal CA1 region) in 5xFAD mice compared with vehicle treatment (Fig. 1F–I).

To further investigate the effects of CA140 on Aβ plaque number with or without formic acid, 8-month-old 5xFAD mice were injected with CA140 (30 mg/kg, i.p.) or vehicle (10% DMSO) daily for 14 days, and brain sections were pretreated with 70% formic acid before immunostaining with an anti-$Aβ_{17-24}$ (4G8) antibody. Consistent with the findings in Fig. 1, CA140 treatment significantly reduced the number of Aβ plaques in the cortex, and immunostaining was not affected by pretreatment with formic acid (Supplementary Fig. 1). Taken together, these data imply that CA140 interacts with aggregated Aβ to reduce Aβ fibril formation, Aβ levels, and Aβ plaque number in vitro and/or in aged 5xFAD mice.

Since CA140 reduced Aβ fibrillation and Aβ plaque number, we further examined the effects of CA140 on tau fibril formation using the ThT fluorescence assay. In this study, we used 2N4R tau, a 441-amino-acid tau protein that is the largest human tau isoform. In the absence of CA140, the ThT fluorescence intensity of 30 μM tau increased rapidly after a lag phase of ~2 h and reached a plateau at ~4 h (Fig. 1J, K), indicating nucleation-dependent tau fibril formation. Treatment with CA140 (5 or 20 molar equivalents) decreased ThT intensity (Fig. 1J, K), indicating that CA140 inhibits 2N4R tau fibril formation.

We then investigated whether CA140 affects tau hyperphosphorylation in aged 5xFAD mice. Eight-month-old 5xFAD mice were injected with vehicle (10% DMSO) or CA140 (30 mg/kg, i.p.) daily for 14 days, and immunostaining of brain slices was performed with an anti-AT100 antibody, which detects tau that is hyperphosphorylated at Thr212/Ser214. Compared with vehicle treatment, CA140 treatment significantly reduced tau hyperphosphorylation at Thr212/Ser214 in the hippocampal CA1 and DG regions (Fig. 1L, M). These data indicate that CA140 inhibits tau fibril formation and downregulates tau phosphorylation in an aged AD mouse model.

(See figure on next page.)

Fig. 1 CA140 reduces Aβ/tau aggregate formation, Aβ levels, and AD pathology in vitro and in vivo. **A** Graph of fluorescence intensity versus concentration of CA140 in the presence of aggregated Aβ42 (average fluorescence measurements from three independent experiments). **B** Real-time monitoring of the inhibitory effects of CA140 on amyloid formation. **C** Quantification of the ThT intensity of Aβ42 at the final time point. **D**, **E** Aβ levels in primary cortical neurons and APP-overexpressing CHO cells. **F–I** Eight-month-old 5xFAD mice were injected with vehicle (10% DMSO) or CA140 (30 mg/kg) daily for 14 days, and immunofluorescence (IF) staining of brain slices was conducted with an anti-$Aβ_{17-24}$ (4G8) antibody (n = 16 brain slices from 4 mice/group). **J**, **K** Quantification of the ThT intensity of 2N4R full-length tau at the final time point. **L**, **M** 8-month-old 5xFAD mice were injected with vehicle (10% DMSO) or CA140 (30 mg/kg, i.p.) daily for 14 days, and IF staining of brain slices was conducted with an anti-$Tau^{Thr212/Ser214}$ (AT100) antibody (Veh, n = 18 brain slices from 4 mice; CA140, n = 20 brain slices from 4 mice). Scale bar = 200 μm. *$p < 0.05$, **$p < 0.01$

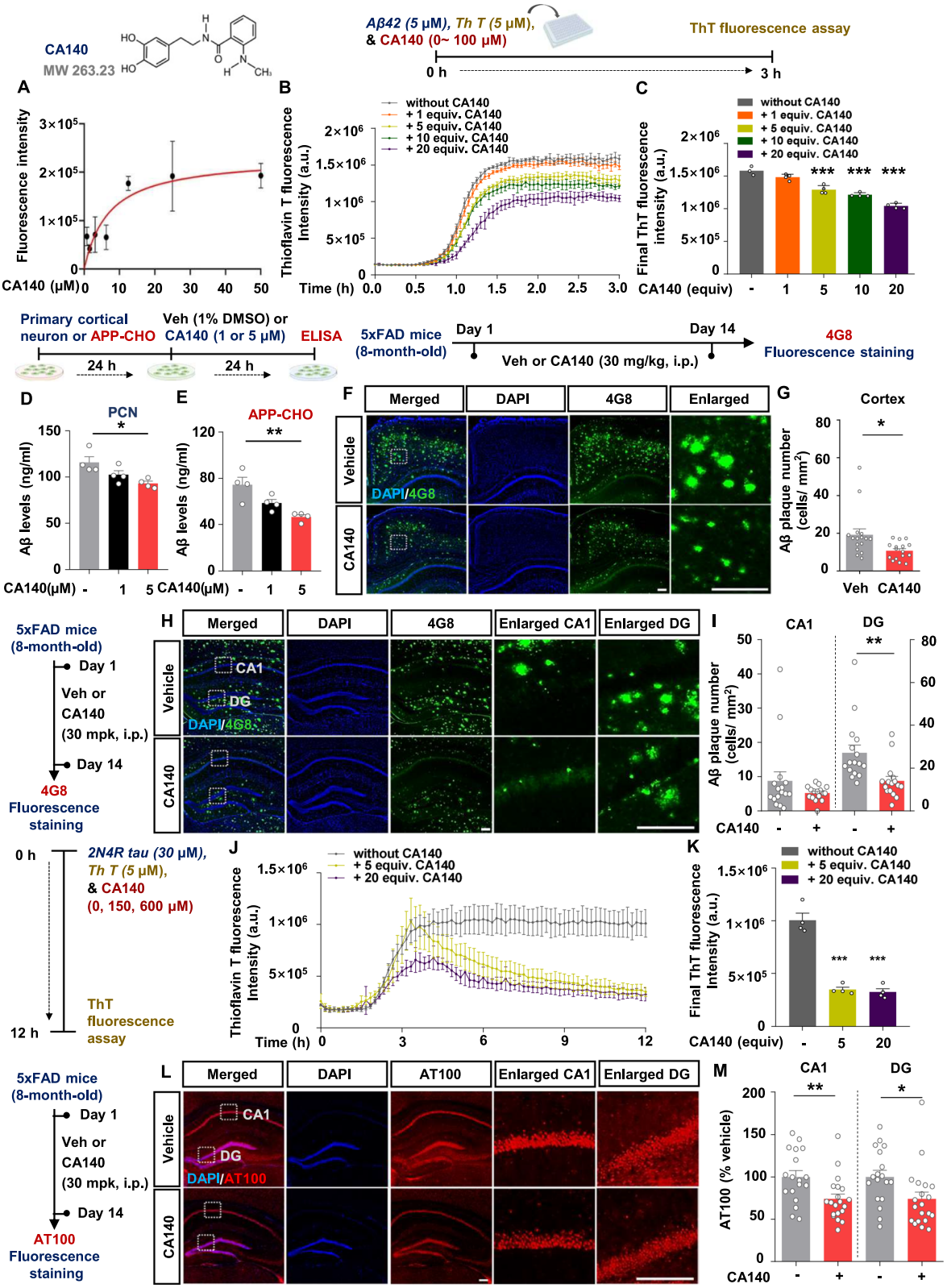

Fig. 1 (See legend on previous page.)

CA140 downregulates genes involved in neuroinflammation in a mouse model of AD

We previously reported that CA140 has anti-inflammatory effects on LPS-evoked neuroinflammation in WT mice and in 3-month-old 5xFAD mice (a model of the early phase of AD in which the neuroinflammatory response occurs) [17]. To extend these findings, we performed RNA sequencing to investigate the molecular mechanism by which CA140 inhibits neuroinflammatory responses in 3-month-old 5xFAD mice. Three-month-old 5xFAD mice were injected with vehicle (10% DMSO) or CA140 (30 mg/kg, i.p.) daily for 14 days. The hippocampus was dissected, and RNA sequencing was performed. By comparing mRNA expression profiles, we identified 822 differentially expressed genes (DEGs), including 183 upregulated and 639 downregulated genes, in CA140-injected 5xFAD mice compared with vehicle-injected 5xFAD mice (Fig. 2A, B and Table S2). Notably, CA140 treatment downregulated several glial cell-specific marker genes in 3-month-old 5xFAD mice (Fig. 2B): *iba1* for microglia, *gfap* for astrocytes, *cxcl10* for AD-associated RAs, *trem2* and *grn* for MGnDs, *clec7a* and *itgax* for DAMs, and *c1qa* and *cr3* for interactions between RAs and DAMs (Fig. 2A, B, E and Table S2). In addition, we found that CA140 treatment significantly reduced the mRNA levels of *cd68* (a marker of M1 microglia) and *gbp2* (a marker of A1 astrocytes) in this mouse model of the early phase of AD (Fig. 2B, E).

To further examine the cellular processes affected by CA140, we performed enrichment analysis of the up- or downregulated DEGs using DAVID software [34]. The DEGs that were downregulated by CA140 treatment in 5xFAD mice were strongly associated with pathways related to the inflammatory response (cytokine production, TLR, RIG-like/NOD, NF-κB, and Nlrp3 inflammasome signaling pathways) and glial cell activation/proliferation (Fig. 2C, E and Table S3A). By contrast, the DEGs that were upregulated by CA140 treatment in 5xFAD mice were mainly associated with pathways related to synaptic function in the hippocampus (learning or memory, cognition, synaptic signaling, and cAMP/calcium signaling pathways) (Fig. 2D and Table S3B).

To validate the RNA sequencing results, we performed real-time PCR and confirmed that representative inflammatory response-related molecules (*nlrp3* and *il1β*) and glial cell markers (*iba-1* and *gfap*) were downregulated in CA140-injected 5xFAD mice (Fig. 2F).

To visualize the collective actions of CA140 in this mouse model of AD, we constructed a network model describing the interactions among the downregulated inflammatory response-related genes based on interaction information in the KEGG pathway database and WikiPathways [35, 36]. The network model suggested that CA140 downregulates TLR1/4-dependent signaling, which is followed by inhibition of the downstream NF-κB and IRF5/7 signaling pathways that produce proinflammatory cytokines/chemokines and Nlrp3 inflammasome-mediated cytokine production (Fig. 2G). These data suggest that CA140 reduces neuroinflammatory responses through NLRP3 in 3-month-old 5xFAD mice.

CA140 downregulates microglial/astrocyte activation in 8-month-old 5xFAD mice

Neuroinflammation is closely associated with Aβ/tau pathology in AD mouse models and patients with AD and is predominantly regulated by glial cells [38, 39]. Since CA140 downregulated neuroinflammatory responses in a mouse model of the early phase of AD (3-month-old 5xFAD mice), we examined whether CA140 regulates neuroinflammatory-associated glial activation in an aged AD mouse model. Eight-month-old 5xFAD mice were injected with CA140 (30 mg/kg, i.p.) or vehicle (10% DMSO) daily for 14 days, and IF staining was conducted with anti-Iba-1 (a microglial marker) and anti-GFAP (an astrocyte marker) antibodies. We found that CA140 treatment significantly diminished Iba-1 fluorescence intensity and the number of Iba-1-positive cells in the hippocampal CA1 region but not in the hippocampal

(See figure on next page.)

Fig. 2 Identification of genes affected by CA140 in 3-month-old 5xFAD mice. **A** Heatmap of 183 upregulated and 639 downregulated genes in CA140-injected 5xFAD mice compared with vehicle-injected 5xFAD mice. **B** Volcano plot showing differentially expressed genes (DEGs) in CA140-treated 5xFAD mice. The X- and Y-axes present the $\log_2$-fold-change and $-\log_{10}$ (*p* value), respectively. Red and green dots represent upregulated and downregulated genes, respectively. Gray dots represent genes without significant differences in expression. **C**, **D** Gene ontology biological processes (GOBPs) represented by the downregulated (**C**) and upregulated (**D**) genes. The dotted line indicates the *p* value cutoff used. The number of genes in each biological process is indicated in parentheses. **E** DEGs involved in the inflammatory response, glial cell activation/proliferation, and *Nlrp3* inflammasome signaling. The color bar shows the z-score gradient. **F** Relative mRNA levels of the indicated genes in CA140- or vehicle-treated 5xFAD mice were analyzed by real-time PCR (n = 2 mice/group). **G** Network model describing the interactions among inflammatory response-related signaling pathways. The node colors represent downregulation (green) and no change (yellow) of the corresponding genes in CA140-injected 5xFAD mice. Nodes are arranged and connected according to the activation (arrows) information in the KEGG pathway and WikiPathways databases. Solid and dotted lines denote direct and indirect interactions, respectively. "+p", phosphorylation. "+u", ubiquitination. *$p < 0.05$, **$p < 0.01$

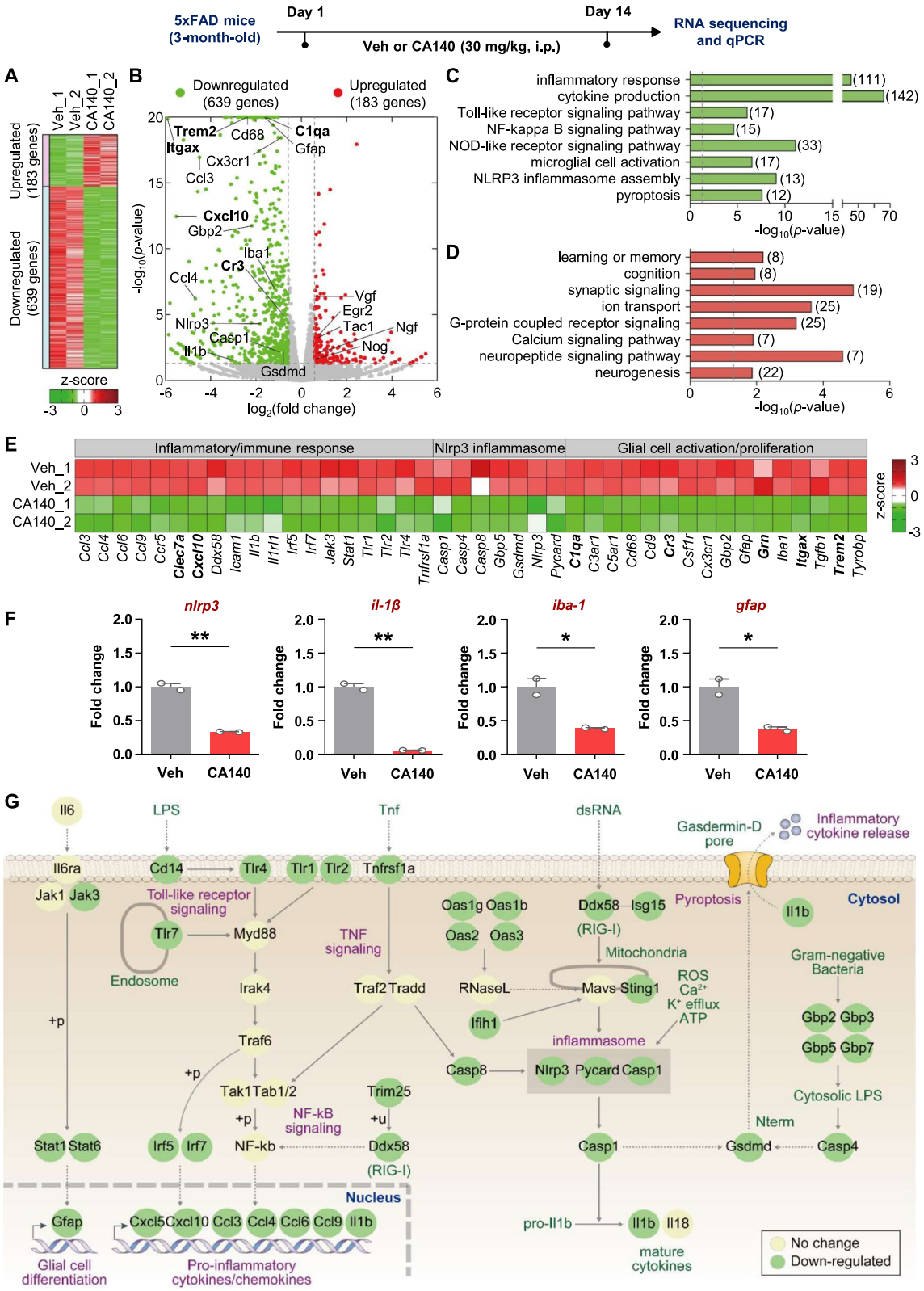

Fig. 2 (See legend on previous page.)

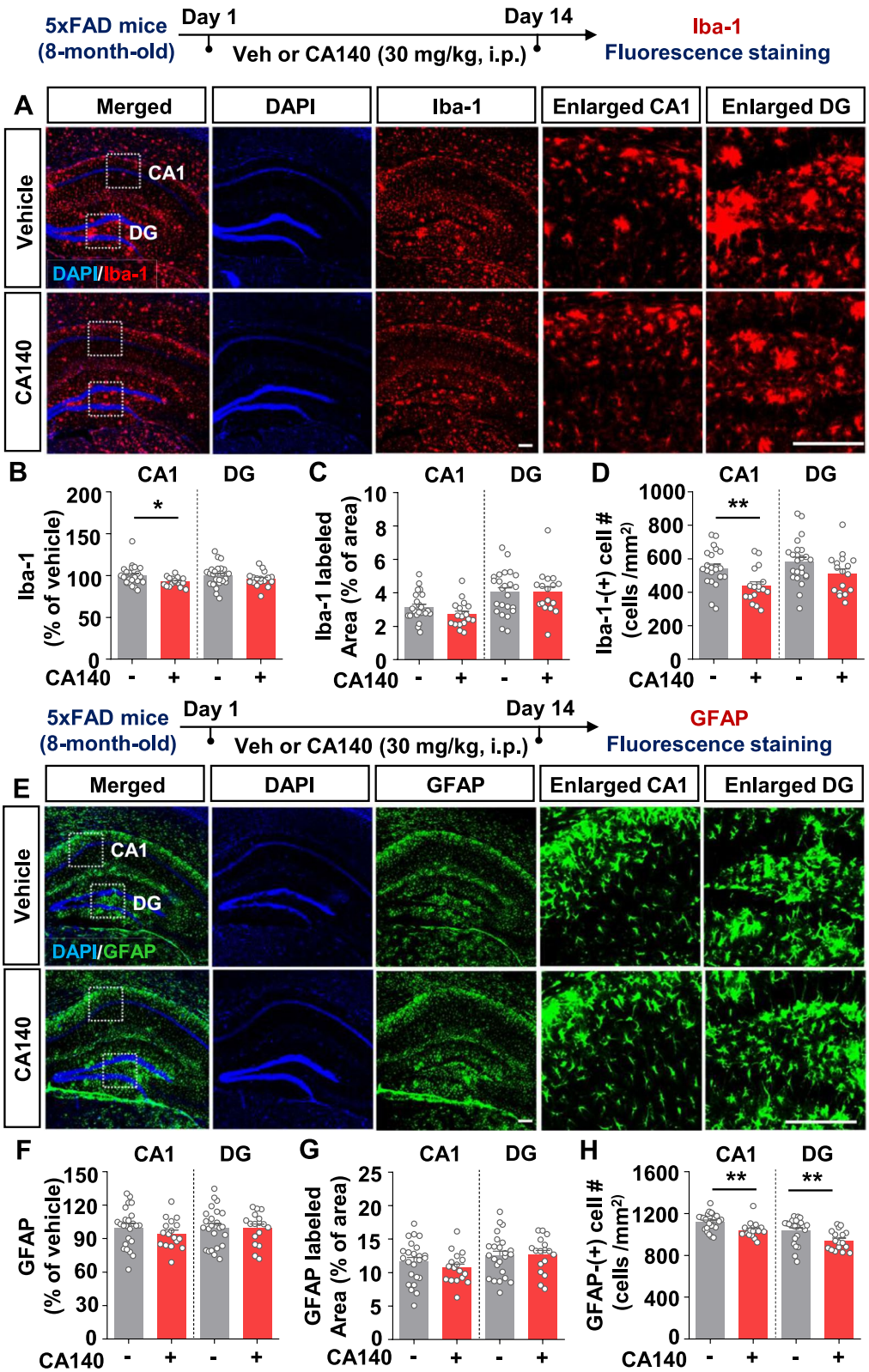

Fig. 3 CA140 injection regulates microglial activation and astrocytic morphology in 8-month-old 5xFAD mice. **A–H** Eight-month-old 5xFAD mice were injected with vehicle (10% DMSO) or CA140 (30 mg/kg, i.p.) daily for 14 days, and immunofluorescence staining of brain slices was conducted with anti-Iba-1 and anti-GFAP antibodies (Iba-1: Veh, n = 23–24 brain slices from 4 mice; CA140, n = 17 brain slices from 4 mice; GFAP: Veh, n = 24 brain slices from 4 mice; CA140, n = 17 brain slices from 4 mice). Scale bar = 200 μm. *$p < 0.05$, **$p < 0.01$

DG region (Fig. 3A–D). In addition, CA140 treatment only significantly decreased the number of GFAP-positive cells in the hippocampus and had no effect on GFAP fluorescence intensity or the GFAP-positive area (Fig. 3E–H). These results demonstrate that CA140 also suppresses neuroinflammatory responses in an aged AD mouse model and that this suppression occurs via the downregulation of microglial and astrocyte activation.

CA140 downregulates neuroinflammatory responses and AD-associated reactive gliosis in 8-month-old 5xFAD mice

A recent study found that the induction of neuroinflammation by proinflammatory cytokines, including IL-1β, is activated by NLRP3 inflammasome formation in the brain in 5xFAD mice [40]. Our real-time PCR analysis demonstrated that CA140 treatment significantly reduced *nlrp3* and *il-1β* mRNA levels in the brain in 3-month-old 5xFAD mice (Fig. 2). We therefore examined whether CA140 modulates NLRP3 expression to downregulate neuroinflammatory responses in an aged AD mouse model. Eight-month-old 5xFAD mice were injected with CA140 (30 mg/kg, i.p.) or vehicle (10% DMSO) daily for 14 days, and IF staining was conducted with anti-NLRP3 and anti-IL-1β antibodies. Compared with vehicle, CA140 significantly reduced NLRP3 levels in the hippocampus in 8-month-old 5xFAD mice (Fig. 4A, C). In addition, CA140 treatment significantly reduced the levels of the proinflammatory cytokine IL-1β in the hippocampus in 5xFAD mice (Fig. 4B, D).

Since we observed that CA140 treatment diminished microglial/astrocyte activation and proinflammatory cytokine IL-1β and NLRP3 levels in a mouse model of AD, we assessed the effects of CA140 on neuroinflammatory dynamics and the functional states of neuroinflammatory responses in vivo. For this experiment, 8-month-old 5xFAD mice were injected with CA140 (30 mg/kg, i.p.) or vehicle (10% DMSO) daily for 14 days, and IF staining was conducted with anti-CXCL10 and anti-C1QA antibodies. We found that CA140 treatment significantly reduced the expression of CXCL10 (a marker of RAs) and C1QA (a marker of interactions between RAs and DAMs) in the hippocampus in 5xFAD mice (Fig. 4E–H). We also examined the effects of CA140 on M1/M2 and A1/A2 polarization states in this aged AD mouse model and found that CA140 treatment did not alter the mRNA expression of GBP2 (a marker of A1 astrocytes), CD68 (a marker of M1 microglia), and CD206 (a marker of M2 microglia) in 5xFAD mice (Supplementary Fig. 2).

Taken together, these results reveal that CA140 inhibits its neuroinflammatory responses by suppressing NLRP3 activation and reactive gliosis in an aged AD mouse model.

CA140 decreases reactive gliosis in primary astrocytes and primary microglia from 5xFAD mice

PACs and PMCs were used to investigate the effect of CA140 on a broad spectrum of astroglial/microglial reactive states, including AD-associated RAs [41, 42], homeostatic microglia, MGnDs, DAMs, PAMs, and LDAMs [43, 44]. For this experiment, mixed glial cells prepared from whole brains of postnatal day 1–2 5xFAD pups were cultured for 3 weeks. Then, PACs and PMCs were isolated and treated with vehicle (1% DMSO) or CA140 (5 μM) for 24 h, and real-time PCR was conducted. We found that CA140 treatment significantly decreased the mRNA levels of *s100β* (a cell signaling marker of AD-associated RAs) and *cxcl10* (a secreted protein marker of AD-associated RAs) in PACs from 5xFAD mice (Fig. 5A, B). However, CA140 treatment did not alter the mRNA levels of metabolism, cytoskeleton, or chaperone markers of AD-associated RAs in PACs from 5xFAD mice (Fig. 5C–E). In addition, CA140 significantly reduced the mRNA levels of *cr3* and *c1qa* (markers of the interactions of RAs and DAMs) in PACs from 5xFAD mice (Fig. 5F). These data suggest that CA140 alters neuroinflammatory responses by modulating the expression of cell signaling and secreted protein markers of AD-associated RAs and markers of the interactions of RAs and DAMs in PACs from 5xFAD mice (Fig. 5G).

In PMCs from 5xFAD mice, CA140 treatment significantly increased the mRNA levels of *cx3cr1* and *p2ry12* (markers of homeostatic microglia) (Fig. 5H). Interestingly, in PMCs from 5xFAD mice, CA140 treatment significantly downregulated the mRNA levels of a marker of PAMs, *gpnmb* whose level was also increased in the MGnDs (Fig. 5I) [45]. However, CA140 treatment did not modulate the mRNA levels of markers of DAMs (*itgax, clec7a, lpl, cstd,* and *cd44*) and MGnDs (*apoE, spp1, trem2,* and *grn*) in PMCs from 5xFAD mice (Fig. 5J, K). In addition, CA140 decreased the mRNA levels of *cln3* (a marker of LDAMs) and *cr3* and *c1qa* (markers of interactions of RAs and DAMs) in PMCs from 5xFAD mice (Fig. 5L–N). Collectively, these experiments show that CA140 downregulates reactive gliosis during the neuroinflammatory dynamics of AD pathophysiology and upregulates homeostatic microglial function in PACs and/or PMCs.

CA140 prevents scopolamine (SCO)-induced impairments in long-term memory, dendritic spine number, and LTP in WT mice

To determine whether CA140 regulates cognitive and synaptic function under pathological conditions, we

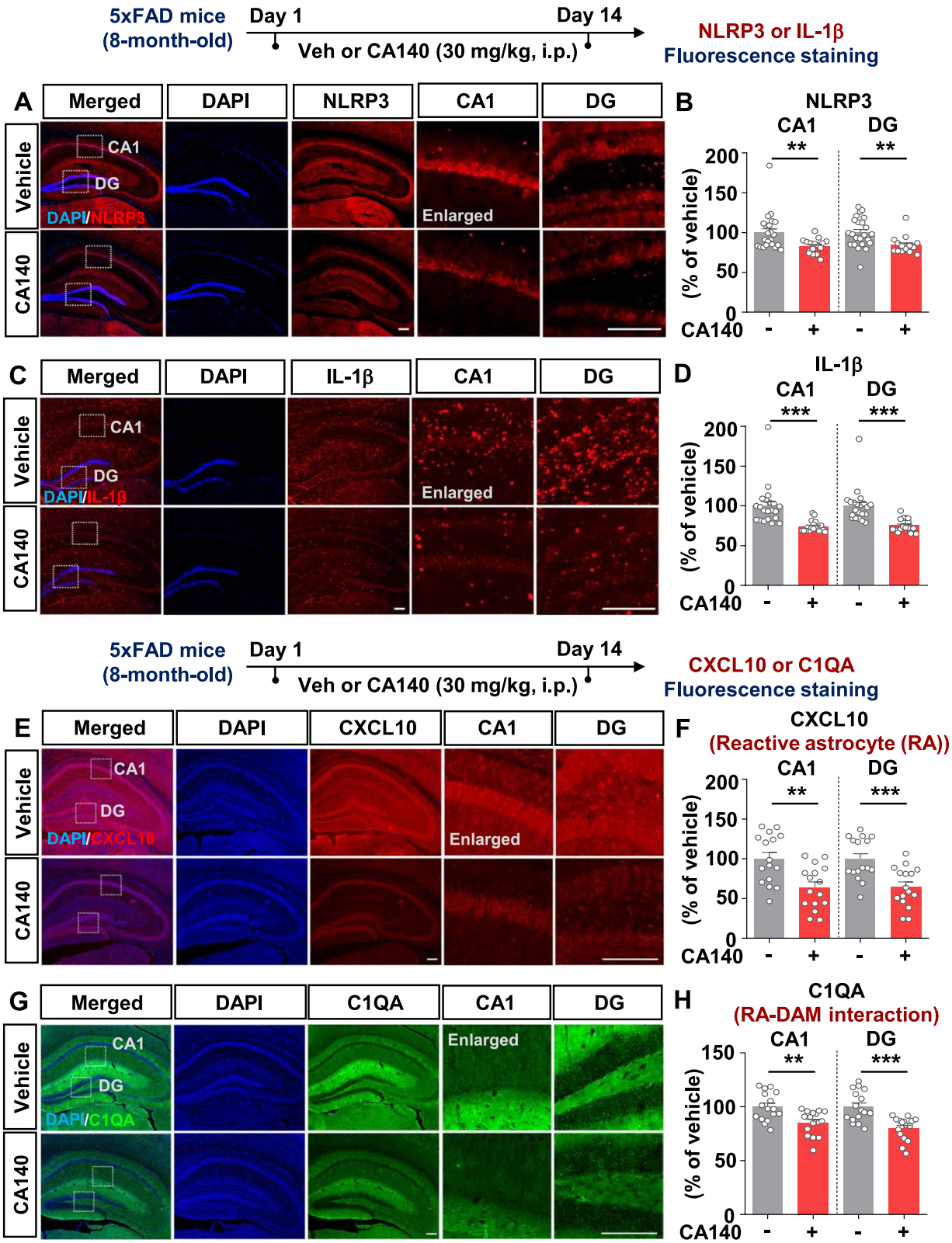

Fig. 4 CA140 administration reduces NLRP3, IL-1β levels and reactive gliosis in 8-month-old 5xFAD mice. **A–H** Eight-month-old 5xFAD mice were injected with vehicle (10% DMSO) or CA140 (30 mg/kg, i.p.) daily for 14 days, and immunofluorescence staining of brain slices was performed with anti-NLRP3 (**A**, **B**), anti-IL-1β (**C**, **D**), anti-CXCL10 (**E**, **F**) and anti-C1QA (**G**, **H**) antibodies (n = 16–23 brain slices from 4 mice). Scale bar = 200 μm. *$p < 0.05$, **$p < 0.01$, ***$p < 0.001$

used a model of amnesia induced by scopolamine (SCO), a muscarinic acetylcholine receptor antagonist that is involved in hippocampal LTP reduction and memory impairment [46, 47]. WT mice were injected with CA140 (30 mg/kg, i.p.) or vehicle (10% DMSO) daily for 14 days. On days 3 to 14, the mice were also injected with SCO (1 mg/kg, i.p.) or PBS daily. Behavior experiments were performed on days 12 to 14. Interestingly, compared with vehicle treatment, SCO treatment significantly impaired long-term memory but had no effect on short-term spatial memory in WT mice (Fig. 6A, B). Importantly, CA140 treatment rescued SCO-induced long-term memory deficits in WT mice but did not affect short-term memory (Fig. 6A, B).

To demonstrate the molecular mechanisms by which CA140 improves cognitive function, the effects of CA140 on dendritic spine formation, basal transmission, and LPT in SCO-injected WT mice were analyzed. First, to determine whether CA140 modulates dendritic spine formation in SCO-treated WT mice, Golgi staining was performed. Dendritic spine density in the hippocampal basal shaft (BS), cortical apical oblique (AO) and cortical BS region was significantly reduced in SCO-treated WT mice compared with vehicle-treated WT mice (Fig. 6C–E). CA140 treatment restored hippocampal and cortical dendritic spine numbers in SCO-treated WT mice (Fig. 6C–E), indicating that CA140 rescues SCO-mediated dendritic spine loss in WT mice.

Second, to examine the potential recovery effect of CA140 treatment on hippocampal LTP, WT mice were injected with vehicle (10% DMSO) or CA140 (30 mg/kg, i.p.) daily for 14 days and PBS or SCO (1 mg/kg, i.p.) daily on days 3 to 14. Subsequent measurement of basal synaptic transmission in the hippocampus (Fig. 6F–H) and input–output curve analysis showed that basal synaptic transmission at the SC-CA1 pathway was unchanged in SCO-treated WT mice compared to vehicle-treated WT mice. Administration of CA140 to SCO-treated WT mice also had no effect on basal synaptic transmission (Fig. 6F–H). However, consistent with previous findings [32, 33], SCO treatment suppressed LTP induction at SC-CA1 synapses in WT mice (Fig. 6I–M). More importantly, CA140 treatment fully reversed LTP attenuation in SCO-treated WT mice (Fig. 6I–M). These results demonstrate that CA140 significantly reduces the inhibition of LTP by SCO in vivo.

CA140 restores long-term memory, dendritic spine number, LTP, and synaptic function in aged 5xFAD mice

Given the positive effects of CA140 on cognitive function, dendritic spine number, and LTP in the SCO-mediated amnesia mouse model, we further investigated the effects of CA140 on synaptic/cognitive function in an aged AD mouse model. Eight-month-old 5xFAD mice were injected with vehicle (10% DMSO) or CA140 (30 mg/kg, i.p.) daily for 17 days, and Y-maze and NOR tests were conducted on days 15 to 17. Strikingly, CA140 treatment increased the object preference (%) in the NOR test but not alternation triplets (%) in the Y-maze test compared with vehicle treatment (Fig. 7A, B). These results indicate that CA140 improves long-term memory deficits in aged 5xFAD mice.

To further explore the memory-improving effects of CA140 in 8-month-old 5xFAD mice, we assessed whether CA140 modulates dendritic spine formation, which is associated with cognitive function [48]. In 8-month-old 5xFAD mice, CA140 treatment significantly increased dendritic spine number in the hippocampal AO and BS region (Fig. 7C, D) and cortical AO region but not in the cortical BS (Supplementary Fig. 3). These data indicate that CA140 improves long-term memory and dendritic spine formation in aged 5xFAD mice.

Cognitive function is closely associated with hippocampal synaptic strength, and 5xFAD mice that are older than 6 months exhibit memory dysfunction and attenuated LTP compared with WT mice [49, 50]. We therefore examined the effect of CA140 on LTP induction in 8-month-old 5xFAD mice and found that CA140 tended to increase LTP, although not significantly (Fig. 7E–G). Taken together, these results demonstrate that CA140 ameliorates impairments in cognitive dysfunction, dendritic spine density, and LTP in an aged AD mouse model.

To further investigate the effects of CA140 on synaptic function in 5xFAD mice, 6-month-old 5xFAD mice were injected with vehicle (10% DMSO) or CA140 (30 mg/kg, i.p. for consecutive 14 days); then, mEPSCs were monitored. We found that CA140 treatment

(See figure on next page.)

Fig. 5 CA140 treatment regulates reactive gliosis in primary astrocytes (PACs) and primary microglia (PMC) from 5xFAD mice. **A–F** PACs from 5xFAD mice were treated with vehicle (1% DMSO) or CA140 (5 μM) for 24 h, and the relative mRNA levels of the indicated genes were analyzed by real-time PCR (n = 12–15/group). **G** Summary illustration of the regulatory effect of CA140 on reactive astrogliosis in PACs from 5xFAD mice. **H–M** PMCs from 5xFAD mice were treated with vehicle (1% DMSO) or CA140 (5 μM) for 24 h, and the relative mRNA levels of the indicated genes were analyzed by real-time PCR (n = 5–6/group). **N** Summary illustration of the regulatory effect of CA140 on microglial reactive state in PMCs from 5xFAD mice. $^{*}p < 0.05$, $^{**}p < 0.01$, $^{***}p < 0.001$

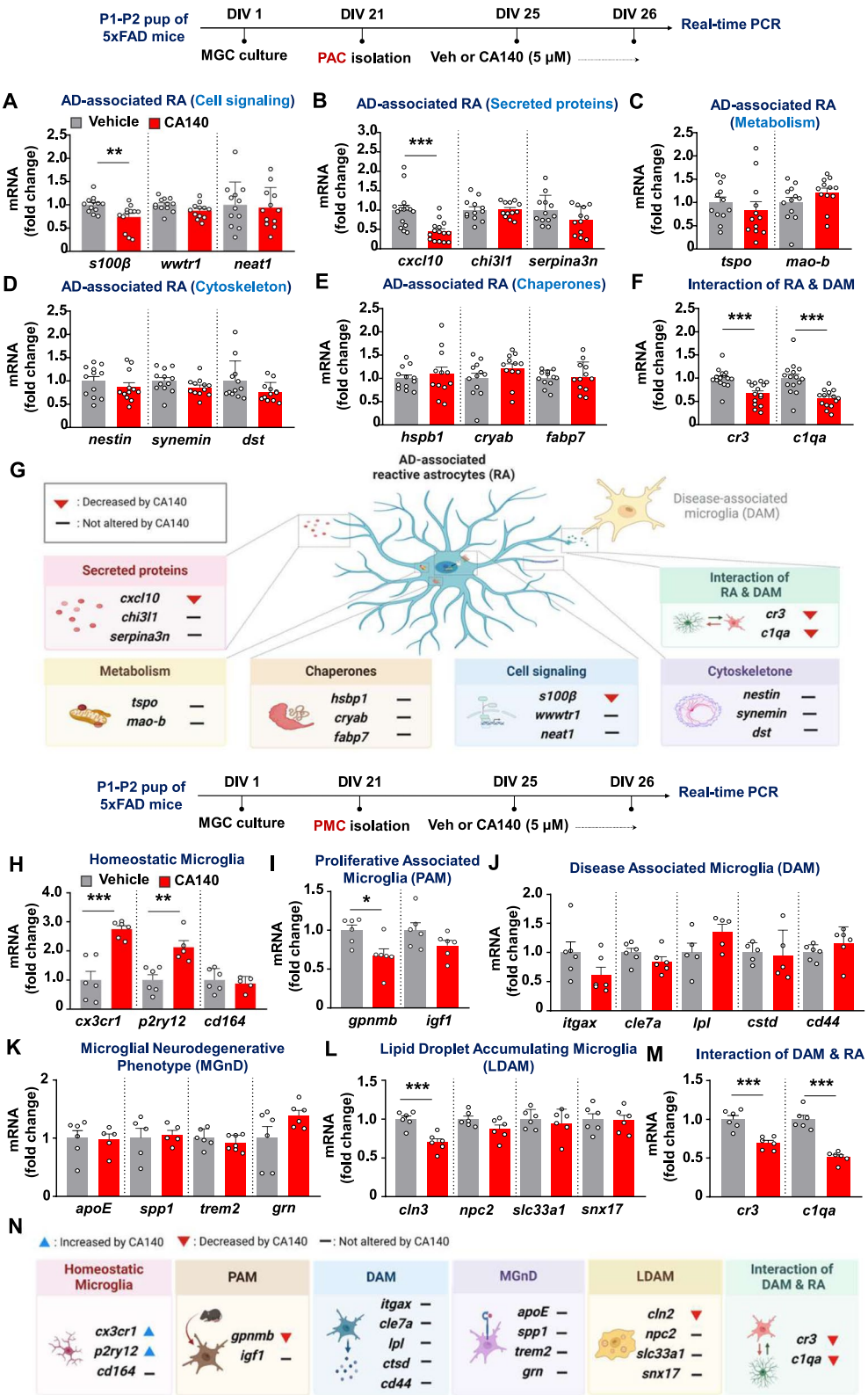

Fig. 5 (See legend on previous page.)

markedly increased the frequency but not the amplitude of mEPSCs in 6-month-old 5xFAD mice (Fig. 7H–J). These data indicate that CA140 treatment may facilitate presynaptic function or increase the number of synapses to alter synaptic and cognitive function in aged 5xFAD mice (Fig. 7H–J).

We then examined whether CA140 modulates presynaptic and postsynaptic protein expression to rescue cognitive and synaptic function in aged 5xFAD mice. For this experiment, eight-month-old 5xFAD mice were injected with vehicle (10% DMSO) or CA140 (30 mg/kg, i.p.) daily for 14 days, and IF staining was conducted with anti-synaptophysin and anti-PSD-95 antibodies. We found that CA140 treatment significantly increased synaptophysin expression in the hippocampal CA1 region in 8-month-old 5xFAD mice (Fig. 7K–L). However, CA140 treatment did not alter PSD-95 expression in the hippocampal CA1 region in 8-month-old 5xFAD mice (Fig. 7M, N). These data indicate that CA140 improves presynaptic performance in aged 5xFAD mice to restore cognitive and synaptic function.

CA140 improves cognitive function through DRD1 signaling in 8-month-old 5xFAD mice

We previously demonstrated that the DA analogue CA140 suppresses the LPS-evoked inflammatory response via modulating DRD1 in BV2 microglial cells [17]. Here, we followed up on this finding by testing whether CA140 acts as an agonist or antagonist of DRD1. HEK293 cells were transfected with DRD1 plasmid DNA for 48 h, pretreated with a LE300 (10 μM, DRD1 antagonist) or vehicle (1% DMSO) for 30 min, and finally treated with A77636 (5 μM, DRD1 agonist), DA (10 or 100 μM), or CA140 (10, 50, or 100 μM) for 1 h. Subsequent cAMP ELISA analysis showed that treatment with A77636, DA, or CA140 significantly increased cAMP levels compared with vehicle treatment (Fig. 8A). However, pretreatment with LE300 followed by CA140 treatment (100 μM) did not enhance cAMP levels, suggesting that CA140 increases cAMP levels by acting as a DRD1 agonist (Fig. 8A).

Next, we investigated whether CA140 regulates cognitive function in a DRD1-dependent manner under pathological conditions. Eight-month-old 5xFAD mice were injected with AAV-DRD1 shRNA or AAV-control shRNA in the bilateral hippocampal CA1 regions. Three weeks after AAV injection, the mice were injected with vehicle (10% DMSO) or CA140 (30 mg/kg, i.p.) daily for 14 days, followed by IF staining of brain slices with an anti-DRD1 antibody. We found that treatment with DRD1 shRNA and vehicle significantly reduced DRD1 levels compared with treatment with control shRNA and vehicle, confirming successful DRD1 shRNA infection in the hippocampal CA1 region in aged 5xFAD mice (Fig. 8B, C). Cognitive behavioral tests (Y-maze and NOR) were then performed. Consistent with the findings presented in Fig. 7A, neither treatment with control shRNA and CA140 nor treatment with DRD1 shRNA and CA140 affected short-term memory compared with treatment with control shRNA and vehicle (Fig. 8D). However, treatment with control shRNA and CA140 improved long-term memory compared with treatment with control shRNA and vehicle (Fig. 8E). More importantly, treatment with DRD1 shRNA and CA140 did not improve long-term memory compared with treatment with DRD1 shRNA and vehicle (Fig. 8E). These data indicate that CA140 enhances cognitive function through DRD1 in an aged AD mouse model.

We further investigated the molecular mechanisms by which CA140 improves cognitive function under pathological conditions. Because CaMKIIα/ERK/ELK-1 signaling is closely associated with dendritic spine formation and synaptic plasticity [51–53], we examined whether CA140 modulates downstream CaMKIIα/ERK/ELK-1 signaling in a DRD1-dependent manner in aged 5xFAD mice. For this experiment, 8-month-old 5xFAD

(See figure on next page.)

Fig. 6 CA140 treatment reverses scopolamine (SCO)-induced impairments in long-term memory, dendritic spine number, and LTP in wild-type (WT) mice. **A**, **B** WT mice were injected daily with vehicle (10% DMSO) or CA140 (30 mg/kg, i.p.) for 14 days. On days 3–14, the mice were also injected daily with PBS or SCO (1 mg/kg, i.p.). Y-maze and NOR tests were performed on days 12 and 14, respectively (n = 8 mice/group). **C–E** Representative AO and BS dendrites from the hippocampal CA1 region and cortical layer V region of mice treated with CA140 and/or SCO (hippocampus AO: Veh, n = 77 neurons from 8 mice; SCO, n = 76 neurons from 8 mice; SCO + CA140, n = 76 neurons from 8 mice; hippocampus BS: Veh, n = 76 neurons from 8 mice; SCO, n = 77 neurons from 8 mice; SCO + CA140, n = 76 neurons from 8 mice; cortex AO and BS: n = 24 neurons from 4 mice/group). Scale bar = 10 μm. **F** WT mice were injected daily with CA140 (30 mg/kg, i.p.) or vehicle (10% DMSO) for 14 days and were also injected with SCO (1 mg/kg, i.p.) or PBS on days 3–14. **G** Representative excitatory postsynaptic current (EPSC) traces from the vehicle, SCO, and SCO + CA140 treatment groups. **H** Input–output curves from the vehicle, SCO, and SCO + CA140 treatment groups (Veh, n = 18 cells from 5 mice; SCO, n = 17 cells from 5 mice; SCO + CA140, n = 14 cells from 5 mice). **I** Representative EPSC traces before and after LTP induction in the vehicle, SCO, and SCO + CA140 treatment groups (1: before LTP; 2: after LTP). **J**, **K** Effects of SCO on LTP induction in the presence/absence of CA140. **L** Overlay of the two graphs in **J**, **K**. **M** Summary statistics for LTP induction (last 5 min: Veh, n = 20 cells from 8 mice; SCO, n = 22 cells from 8 mice; SCO + CA140, n = 22 cells from 7 mice). *$p < 0.05$, **$p < 0.01$, ***$p < 0.001$

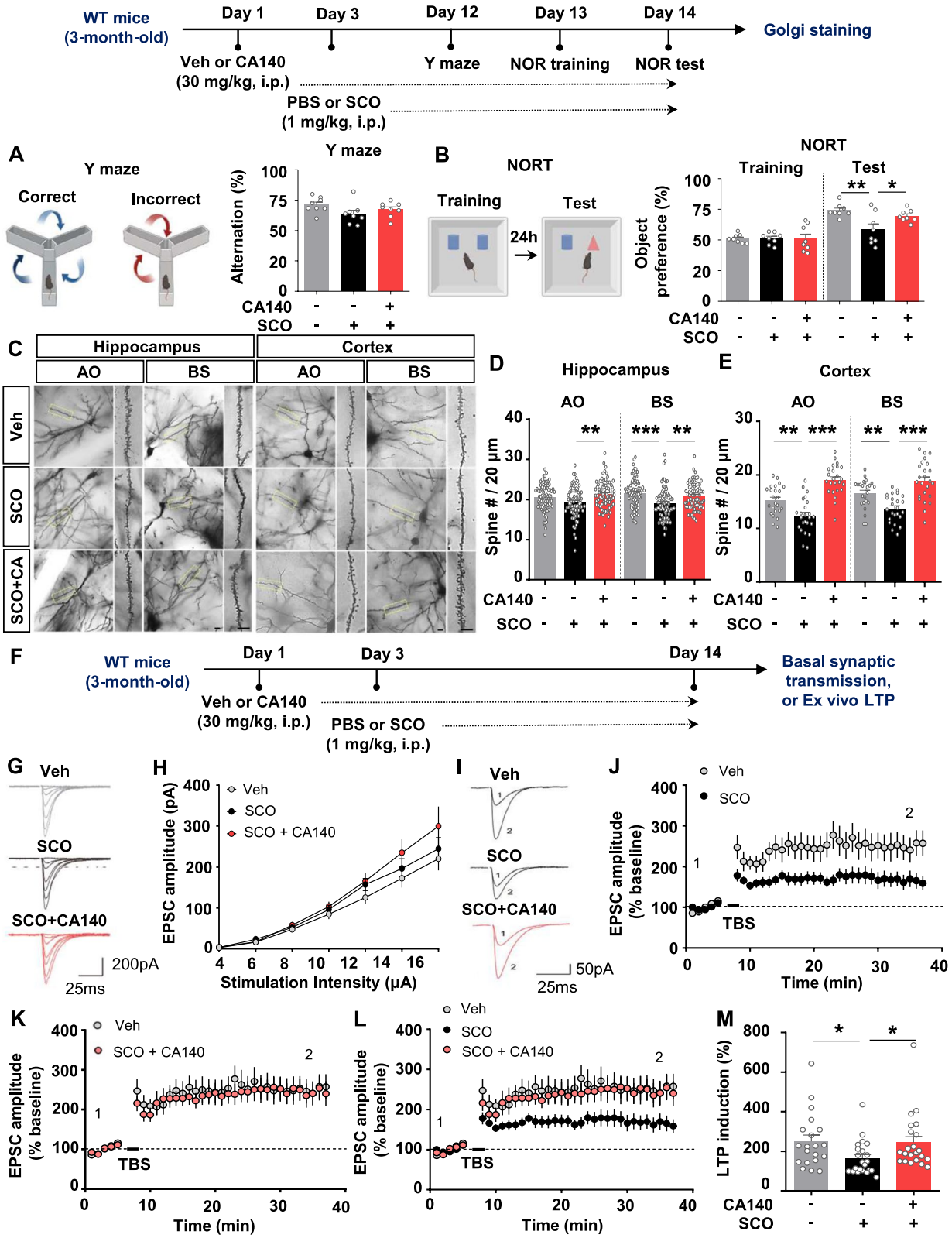

Fig. 6 (See legend on previous page.)

mice were injected with control shRNA or DRD1 shRNA virus into the hippocampal CA1 region. Three weeks after virus injection, the mice were injected with vehicle (10% DMSO) or CA140 (30 mg/kg, i.p.) daily for 17 days. Subsequent western blotting of hippocampal slices showed that treatment with control shRNA and CA140 did not alter p-CaMKIIα and p-ERK levels compared with treatment with control shRNA and vehicle-treated 5xFAD mice (Fig. 8F, G). In addition, treatment with DRD1 shRNA and CA140 did not change p-CaMKIIα and p-ERK levels compared with treatment with DRD1 shRNA and vehicle-treated 5xFAD mice (Fig. 8F, G). By contrast, treatment with control shRNA and CA140 suppressed p-ELK1 levels compared with treatment with control shRNA and vehicle (Fig. 8H), but treatment with DRD1 shRNA and CA140 did not significantly decreased p-ELK1 levels compared with treatment with DRD1 shRNA and vehicle-treated 5xFAD mice (Fig. 8H). These data indicate that the regulatory effect of CA140 on cognitive function is partially regulated by DRD1/Elk-1 signaling in aged 5xFAD mice.

CA140 downregulates Aβ pathology via DRD1 signaling in 8-month-old 5xFAD mice

Since CA140 improved long-term recognition memory through DRD1 signaling under pathological conditions**,** we next examined whether CA140 attenuates Aβ pathology in a DRD1-dependent manner in an aged AD mouse model. Eight-month-old 5xFAD mice were injected with AAV-DRD1 shRNA or AAV-control shRNA in the bilateral hippocampal CA1 region. Three weeks after AAV injection, the mice were administered vehicle (10% DMSO) or CA140 (30 mg/kg, i.p.) daily for 14 days. IF staining of brain slices was then performed with anti-$A\beta_{17\text{-}24}$ (4G8) antibody. Treatment with control shRNA and CA140 significantly reduced Aβ plaque number in 5xFAD mice compared with treatment with control shRNA and vehicle (Fig. 8I, J). More importantly, treatment with DRD1 shRNA and CA140 did not affect Aβ plaque number in 5xFAD mice compared with treatment with DRD1 shRNA and vehicle (Fig. 8I, J). These data indicate that CA140 reduces Aβ pathology by modulating DRD1 signaling under pathological conditions.

CA140 enhances long-term memory and dendritic spine number in WT mice

To examine whether CA140 modulates cognitive and synaptic function under normal conditions, WT mice were injected with vehicle (10% DMSO) or CA140 (30 mg/kg) daily for 7 days and then subjected to Y-maze and novel object recognition (NOR) tests on days 8 to 10. CA140 treatment significantly enhanced the long-term memory but not short-term memory of WT mice compared with vehicle treatment (Fig. 9A, B), indicating that CA140 affects cognitive function in WT mice.

We then investigated whether vehicle (10% DMSO) treatment has specific or non-specific effects on memory function in WT mice. WT mice were injected with water (control for vehicle), 10% DMSO (vehicle), or CA140 (30 mg/kg in 10% DMSO, i.p.) daily for 17 days, and cognitive function was analyzed on days 15 to 17. We found that vehicle treatment did not alter memory function in WT mice compared to water treatment (Supplementary Fig. 4A, B). However, CA140 treatment significantly increased long-term memory in WT mice compared to vehicle treatment (Supplementary Fig. 4A, B). These data suggest that the apparent effects of CA140 treatment on cognitive function in WT mice are not due to effects of vehicle (10% DMSO).

After the behavioral tests, the systemic toxicity of CA140 treatment in WT mice was assessed by western blotting analysis of cleaved caspase-3 expression. CA140 administration did not induce cleaved caspase-3 expression in the liver and kidney, indicating that CA140 does not have in vivo toxicity (Supplementary Fig. 4C, D).

Peripheral inflammation is directly or indirectly associated with adverse effects [54]; thus, we examined whether CA140 treatment influences peripheral proinflammatory

(See figure on next page.)

Fig. 7 CA140 improves long-term memory and dendritic spine number in 5xFAD mice. **A**, **B** Y-maze and NOR tests of 8-month-old 5xFAD mice injected with vehicle (10% DMSO) or CA140 (30 mg/kg, i.p.) daily for 17 days (n = 10 mice/group). **C**, **D** Representative hippocampal AO and BS dendrites of 8-month-old 5xFAD mice injected with vehicle (10% DMSO) or 30 mg/kg CA140 daily for 14 days (AO: Veh, n = 39 neurons from 5 mice; CA140, n = 35 neurons from 5 mice; BS: Veh, n = 35 neurons from 5 mice; CA140, n = 37 neurons from 5 mice). Scale bar = 10 μm. **E** Measurement of LTP in ex vivo hippocampal slices from 8-month-old 5xFAD mice injected with vehicle (10% DMSO) or CA140 (30 mg/kg, i.p.) daily for 14 days. Representative excitatory postsynaptic current (EPSC) traces before and after long-term potentiation (LTP) induction are shown (1: before LTP; 2: after LTP). **F** Effects of CA140 on LTP induction in 8-month-old 5xFAD mice. **G** Summary statistics for LTP induction (last 5 min: Veh, n = 26 cells from 7 mice; CA140, n = 23 cells from 7 mice). **H** Representative traces of mEPSCs of 6-month-old 5xFAD mice injected with vehicle (10% DMSO) or CA140 (30 mg/kg, i.p.) daily for 14 days. **I**, **J** Summary graphs of mEPSC amplitude and frequency in the vehicle and CA140-treated groups (Veh, n = 19 cells from 4 mice; CA140, n = 24 cells from 5 mice). **K**–**N** Eight-month-old 5xFAD mice were injected with vehicle (10% DMSO) or CA140 (30 mg/kg, i.p.) daily for 14 days, and immunofluorescence staining was conducted with anti-synaptophysin (**K**, **L**) or anti-PSD-95 antibodies (**M**, **N**) (n = 16 brain slices from 4 mice/group). Scale bar = 200 μm. *$p < 0.05$, **$p < 0.01$, ***$p < 0.001$

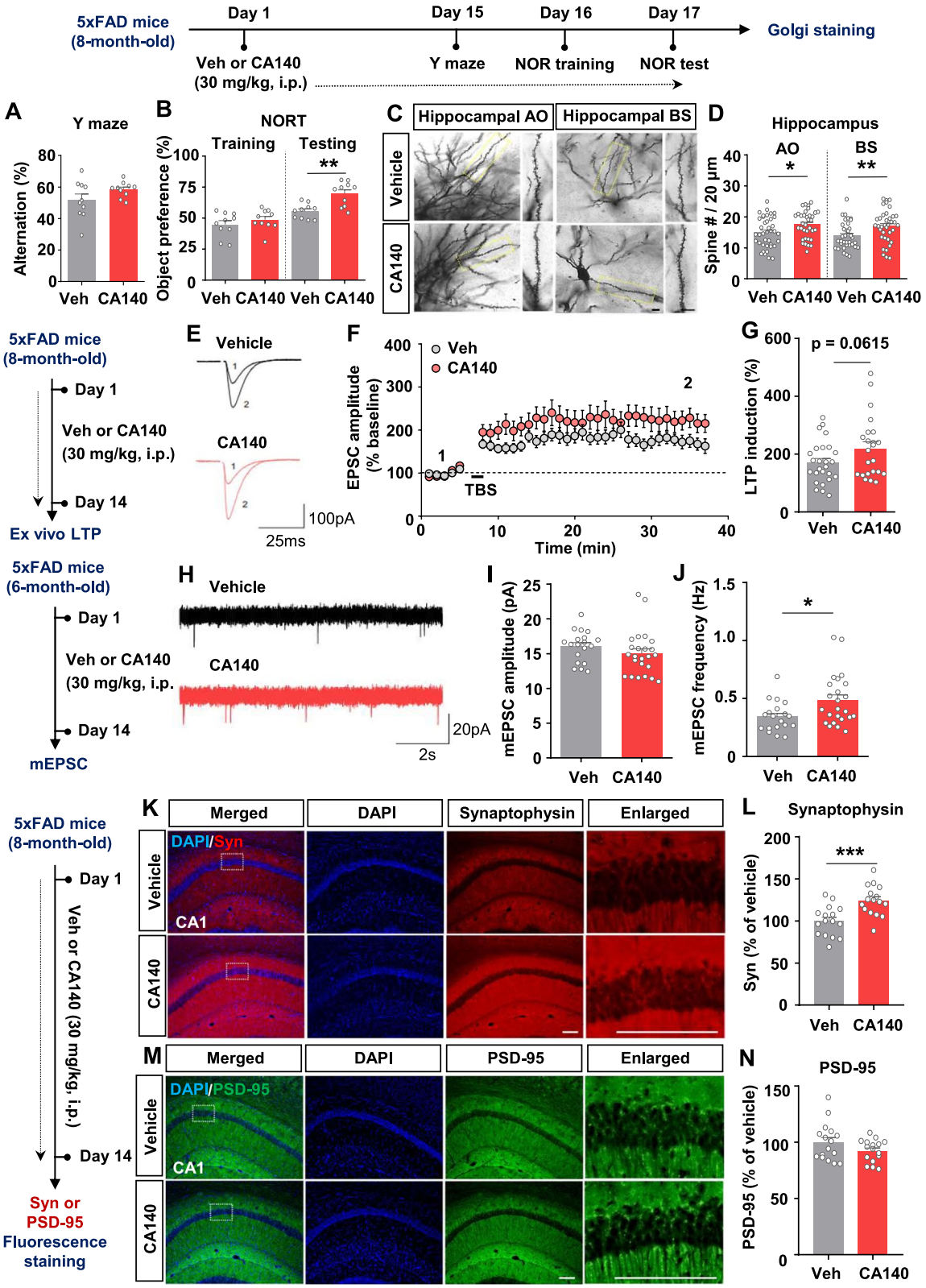

Fig. 7 (See legend on previous page.)

responses under normal conditions. WT mice were injected with water (for comparison with the effects of vehicle on proinflammatory cytokine levels), vehicle (10% DMSO), or CA140 (30 mg/kg in 10% DMSO, i.p.) daily for 17 days, and plasma levels of the proinflammatory cytokines IL-1β and COX-2 were measured. CA140 treatment did not alter plasma IL-1β and COX-2 levels in WT mice compared with water or vehicle (10% DMSO) treatment (Supplementary Fig. 4E, F). These data indicate that chronic administration of CA140 does not induce adverse effects in WT mice.

Finally, to determine whether CA140 improves long-term memory under normal conditions by enhancing dendritic spine density, WT mice were injected with vehicle (10% DMSO) or CA140 (30 mg/kg, i.p.) daily for 10 days, and Golgi staining was performed to measure dendritic spine number in the hippocampus and cortex. Compared with vehicle treatment, CA140 treatment increased dendritic spine number in the hippocampus but not in the cortex in WT mice (Supplementary Fig. 5A-C). These observations suggest that CA140 selectively promotes dendritic spine formation in the hippocampus in WT mice.

DRD1 is essential for the effects of CA140 on cognitive function and dendritic spine density in WT mice

For comparison with the effects of CA140 on cognitive/synaptic function via DRD1 under pathological conditions (Fig. 8), we investigated whether CA140 works with DRD1 to improve long-term memory under normal conditions. WT mice were injected with AAV-DRD1 shRNA or AAV-control shRNA in the bilateral hippocampal CA1 region. One week after AAV injection, the mice were injected with vehicle (10% DMSO) or CA140 (30 mg/kg, i.p.) daily for 17 days. IF staining and behavior experiments (Y-maze and NOR) were conducted on days 15 to 17. We found that DRD1 shRNA treatment reduced DRD1 immunoreactivity in the hippocampal CA1 region in WT mice, confirming successful transduction of AAV-DRD1 shRNA (Fig. 9C).

Consistent with our findings in Fig. 8, treatment with control shRNA and CA140 improved long-term memory but not short-term memory in WT mice compared with treatment with control shRNA and vehicle (Fig. 9D, E). Treatment with DRD1 shRNA and vehicle did not alter short- and long-term memory in WT mice compared with treatment with control shRNA and vehicle (Fig. 9D, E). Importantly, the rescue of long-term memory by CA140 was lost when WT mice were treated with DRD1 shRNA and CA140 (Fig. 9D, E). These findings indicate that CA140 enhances cognitive function through DRD1 under normal conditions.

To demonstrate the molecular mechanisms by which CA140 promotes cognitive function under normal conditions, WT mice were injected with vehicle (10% DMSO) or CA140 (30 mg/kg, i.p.) daily for 17 days. The hippocampus and cortex were dissected, and western blotting was conducted with p-ELK-1, anti-p-CaMKIIα, or anti-p-ERK antibodies. Compared with vehicle treatment, CA140 treatment did not alter pELK-1 levels in the hippocampus and cortex in WT mice (Fig. 9F, G). In addition, a trend of increased p-CaMKIIα levels was observed in the hippocampus but not the cortex in CA140-treated WT mice (Fig. 9H and Supplementary Fig. 6A). Unexpectedly, CA140 treatment did not modulate p-ERK levels in the hippocampus and cortex in WT mice (Fig. 9I and Supplementary Fig. 6B). These data indicate that CA140 treatment upregulates DRD1/CaMKIIα signaling in WT mice.

CA140 increases dendritic spine formation in primary hippocampal neurons

To determine whether CA140 affects dendritic spine formation in vitro, primary hippocampal neurons (PHNs) were transfected with GFP plasmid DNA for 24 h (to visualize dendritic spines) and subsequently treated with CA140 (1 or 5 μM) or vehicle (1% DMSO) for 24 h.

(See figure on next page.)

Fig. 8 CA140 alleviates cognitive function/Aβ pathology through DRD1 signaling in an aged AD mouse model. **A** HEK293 cells were transfected with DRD1 plasmid DNA, pretreated with a DRD1 antagonist (LE300, 10 μM) or vehicle (1% DMSO) for 30 min, and treated with A77636 (5 μM), dopamine (10 or 100 μM), or CA140 (10, 50, or 100 μM) for 1 h. cAMP levels were then measured by ELISA (n = 3/group). **B–E** Eight-month-old 5xFAD mice were injected with AAV-DRD1 shRNA or AAV-control shRNA in the bilateral hippocampal CA1 region. Three weeks after AAV injection, the mice were administered vehicle (10% DMSO) or CA140 (30 mg/kg, i.p.) daily for 14 days, and immunofluorescence staining of brain slices was performed with an anti-DRD1 antibody (n = 16 brain slices from 4 mice/group). Y-maze and NOR tests were performed on days 15–17 (n = 8–9 mice/group) **F–H** 8-month-old 5xFAD mice were injected with AAV-DRD1 shRNA or AAV-control shRNA in the bilateral hippocampal CA1 region. Three weeks after AAV injection, the mice were administered vehicle (10% DMSO) or CA140 (30 mg/kg, i.p.) daily for 17 days, and western blotting of brain lysates was performed with anti-p-Elk1, anti-p-ERK, anti-p-CaMKIIα, or β-actin antibodies (n = 6–8 mice/group). **I, J** Eight-month-old 5xFAD mice were injected with AAV-DRD1shRNA or AAV-control shRNA in the bilateral hippocampal CA1 region. Three weeks after AAV injection, the mice were administered vehicle (10% DMSO) or CA140 (30 mg/kg, i.p.) daily for 14 days, and immunofluorescence staining of brain slices was performed with anti-$A\beta_{17-24}$ (4G8) antibody (n = 16 brain slices from 4 mice/group). Scale bar = 200 μm. *$p < 0.05$, **$p < 0.01$, ***$p < 0.001$

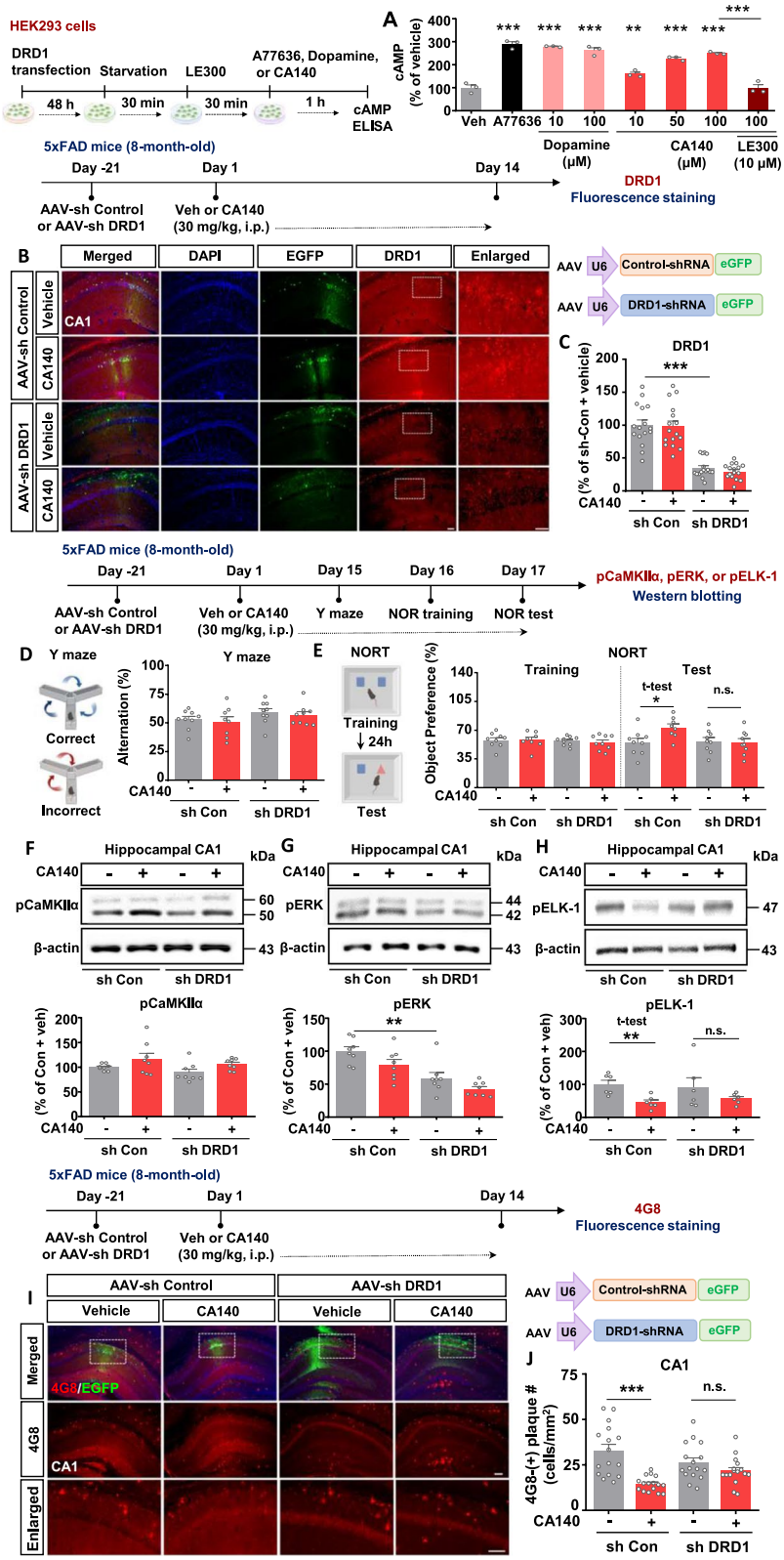

Fig. 8 (See legend on previous page.)

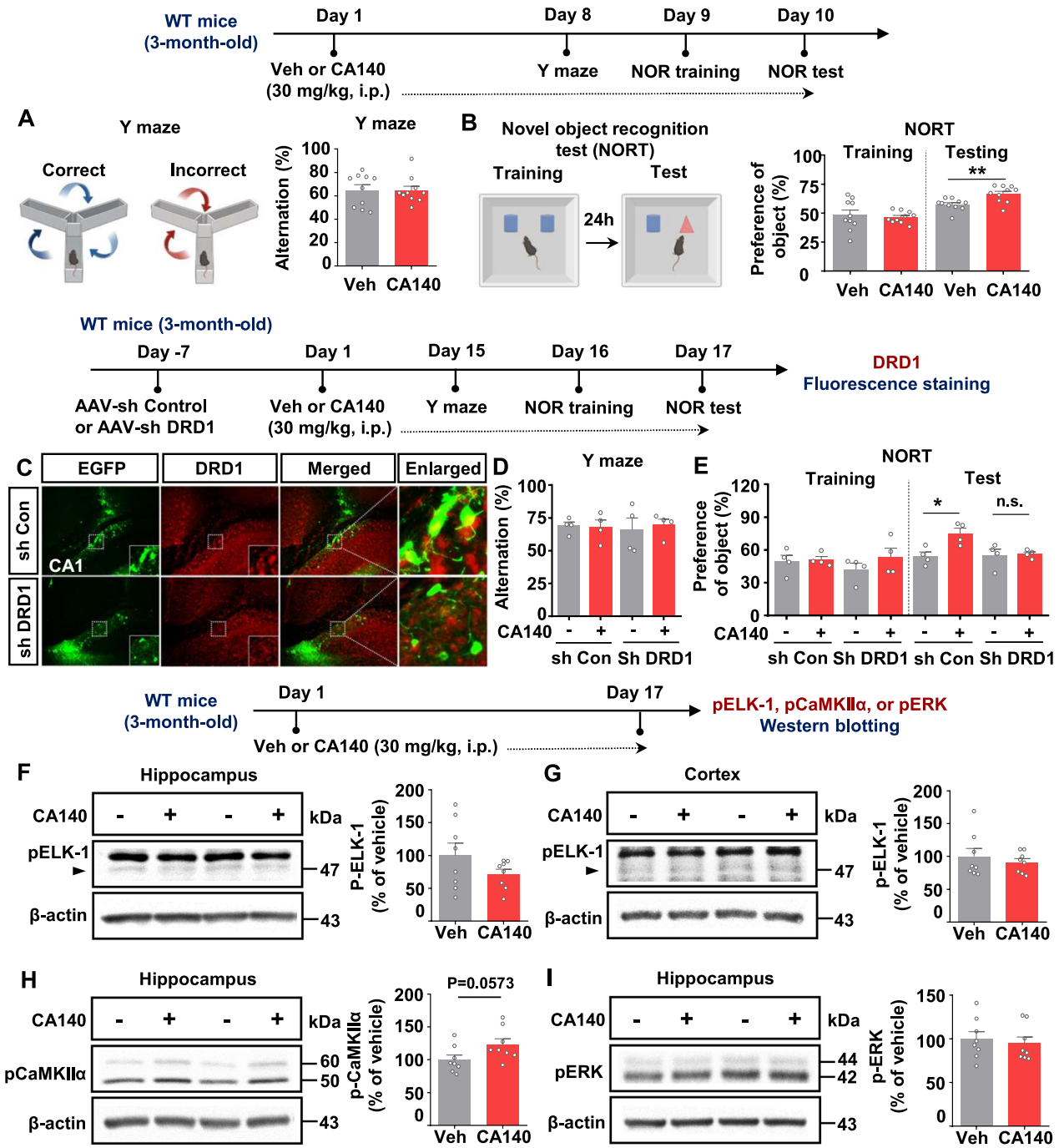

Fig. 9 CA140 modulates DRD1 signaling to alter cognitive and synaptic function in wild-type (WT) mice. **A**, **B** WT mice were injected with vehicle (10% DMSO) or CA140 (30 mg/kg, i.p.) daily for 10 days, and Y-maze and novel object recognition (NOR) tests were conducted (n = 10 mice/group). **C–E** Y-maze and NOR tests of WT mice injected with AAV-Control shRNA or AAV-DRD1 shRNA, followed by daily injections of CA140 (30 mg/kg, i.p.) or vehicle (1% DMSO) for 17 days (n = 4 mice/group). **F–I** WT mice were injected with vehicle (10% DMSO) or CA140 (30 mg/kg, i.p.) daily for 17 days, and western blotting of brain lysates was conducted with anti-p-ELK-1, anti-p-CaMKIIα, or anti-p-ERK antibodies (n = 8 mice/group). *$p < 0.05$, **$p < 0.01$, ***$p < 0.001$

Dendritic spine number was then measured. At 14 days in vitro (DIV14), which corresponds to the peak of synaptogenesis, dendritic spine number was significantly higher in PHNs treated with 1 or 5 μM CA140 than in PHNs treated with vehicle (Fig. 10A, B). In mature neurons (DIV21), treatment with 1 or 5 μM CA140

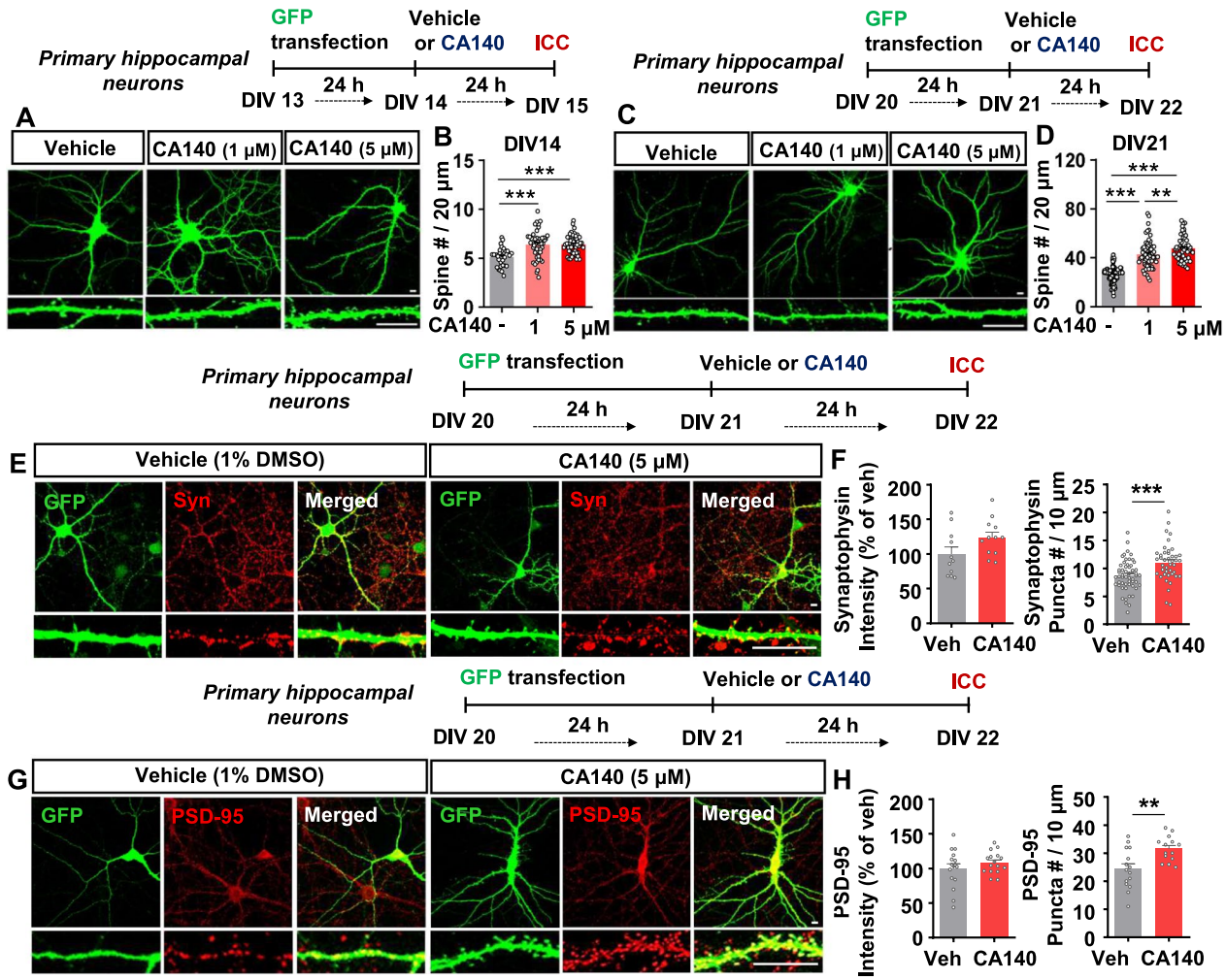

Fig. 10 CA140 enhances dendritic spine formation by regulating functional synapses in primary hippocampal neurons (PHNs). **A**, **C** Dendritic spine density was measured in GFP-transfected PHNs treated with vehicle (1% DMSO) or CA140 (1 or 5 μM) for 24 h on DIV14 and DIV21. **B**, **D** Quantification of data from A and C (DIV14: Veh, n = 30; 1 μM CA140, n = 47; 5 μM CA140, n = 48; DIV21: Veh, n = 161; 1 μM CA140, n = 60; 5 μM CA140, n = 50). **E–H** PHNs were transfected with GFP for 24 h, treated with vehicle (1% DMSO) or CA140 (5 μM) for 24 h, and immunostained with anti-synaptophysin (**E**) or anti-PSD-95 (**G**) antibodies (synaptophysin intensity: Veh, n = 11; CA140, n = 12; synaptophysin puncta number: Veh, n = 55; CA140, n = 42; PSD-95 intensity: Veh, n = 16; CA140, n = 16; PSD-95 puncta number: Veh, n = 15; CA140, n = 14). Scale bar = 20 μm. $^{**}p < 0.01$, $^{***}p < 0.001$

significantly increased dendritic spine number compared with vehicle treatment (Fig. 10C, D). These data indicate that CA140 enhances dendritic spine formation in both developing and mature PHNs.

We then evaluated whether the enhancement in dendritic spine number was correlated with increased excitatory functional synapses in vitro. For this experiment, PHNs were transfected with GFP plasmid DNA for 24 h, treated with vehicle (1% DMSO) or CA140 (5 μM) for 24 h, and immunostained with anti-synaptophysin or anti-PSD-95 antibodies. We found that CA140 treatment significantly enhanced synaptophysin and PSD-95 puncta numbers in PHNs without altering the total levels of synaptophysin and PSD-95 (Fig. 10E–H), suggesting that CA140 increases functional synapses during the mature stages to alter dendritic spine density in PHNs.

CA140 promotes dendritic spine formation through DRD1/CaMKIIα/ERK signaling in primary hippocampal neurons

To examine the effects of the DA analogue CA140 on DRD1 levels in vitro, PHNs were transfected with GFP for 24 h and then treated with vehicle (1% DMSO) or CA140 (5 μM) for 24 h. Immunocytochemistry with an anti-DRD1 antibody showed that CA140 treatment significantly increased DRD1 levels in PHNs compared with vehicle treatment (Fig. 11A, B).

Next, to determine whether DRD1 is required for the positive effects of CA140 on dendritic spine formation in vitro, PHNs were transfected with GFP for 24 h, pretreated with the DRD1 antagonist LE300 (10 μM) or vehicle (1% DMSO) for 1 h, and treated with vehicle (1% DMSO) or CA140 (5 μM) for 23 h. Measurement of dendritic spine number revealed that treatment with LE300 and CA140 eliminated the positive effects of CA140 on dendritic spine formation in PHNs, indicating that CA140 improves dendritic spinogenesis in a DRD1-dependent manner in vitro (Fig. 11C, D).

We then investigated the molecular mechanisms by which CA140 promotes synaptic/cognitive function under normal conditions by assessing the levels of proteins associated with CaMKIIα/ERK signaling, which influences synaptic plasticity and cognitive function by promoting dendritic spine density [55–57]. For this experiment, GFP plasmid-transfected PHNs were treated with vehicle (1% DMSO) or CA140 (5 μM) for 24 h, and immunostaining was conducted with anti-p-CaMKIIα or p-ERK antibodies. We found that CA140 treatment significantly increased the phosphorylation of CaMKIIα and ERK in PHNs (Fig. 11E–H). By contrast, treatment with the DRD1 antagonist LE300 (10 μM) significantly reduced CaMKIIα and ERK phosphorylation in PHNs (Fig. 11I–L).

To determine whether CA140 alters dendritic spine number via CaMKIIα and/or ERK signaling in vitro, PHNs were transfected with GFP for 24 h and pretreated with the CaMKIIα inhibitor KN93 (10 μM), the ERK inhibitor PD98059 (10 μM), or vehicle (1% DMSO) for 1 h. Then, the PHNs were treated with CA140 (5 μM) or vehicle (1% DMSO) for 23 h, and dendritic spine number was measured. Strikingly, pretreatment with KN93 or PD98059 abolished the positive effects of CA140 on dendritic spine number in PHNs (Fig. 11M–P). These data indicate that CA140 modulates DRD1/CaMKIIα/ERK signaling to promote synaptic function in PHNs.

Discussion

Dopamine (DA) release from the predominant DA pathways, namely, the mesocorticolimbic and nigrostriatal pathways, and even from the minor locus coeruleus to dorsal hippocampus pathway is associated with cognitive function and synaptic plasticity [58–62]. Thus, understanding the effects of DA on learning and memory, synaptic strength, and dendritic spinogenesis is critical for developing therapeutic options for the prevention and/or treatment of memory-related diseases, including AD and Parkinson's disease (PD). We previously reported that the DA analogue CA140 reduces neuroinflammatory responses in WT and 3-month-old 5xFAD mice [17]. In the present study, we investigated the effects of CA140 on AD pathology and synaptic and cognitive function and its molecular mechanisms of action under normal and pathological conditions. We found that CA140 directly interacted with aggregated Aβ and decreased Aβ pathology and tau hyperphosphorylation in aged 5xFAD mice. CA140 also mitigated reactive gliosis during the neuroinflammatory dynamics of AD pathophysiology in 5xFAD mice and in PACs and PMCs from 5xFAD mice. In addition, CA140 rescued impairments in long-term memory, mEPSCs, LTP and dendritic spinogenesis in a SCO-mediated model of amnesia in WT mice and in 8-month-old 5xFAD mice. Moreover, CA140 ameliorated AD pathology (including Aβ deposition, tau hyperphosphorylation, and microgliosis) and rescued long-term memory in partial regulated by DRD1/Elk1 signaling in aged 5xFAD mice. Under normal conditions, CA140 promoted synaptic and cognitive function through effects on DRD1/CaMKIIα and/or ERK signaling in WT mice and PHNs. Collectively, our results suggest that CA140 regulates AD pathology, neuroinflammatory responses, and synaptic and cognitive function via DRD1 signaling in WT mice and aged 5xFAD mice.

DA and its derivatives suppress Aβ aggregation and inhibit fibrillation of $Aβ_{40}$ monomers [63, 64]. In addition, DA and its metabolites stabilize neurotoxic Aβ oligomers and reduce Aβ-induced toxicity in vitro [37, 63]. There is also evidence that DA receptors are involved

(See figure on next page.)

Fig. 11 CA140 promotes dendritic spine formation through DRD1/CaMKII/ERK signaling in primary hippocampal neurons (PHNs). **A**, **B** DRD1 levels in GFP-transfected PHNs treated with vehicle (1% DMSO) or CA140 (5 μM) for 24 h were measured by immunostaining with anti-DRD1 antibodies (Veh, n = 152; CA140, n = 155). **C**, **D** Dendritic spine number in GFP-transfected PHNs pretreated with DRD1 inhibitor (LE300, 10 μM) or vehicle (1% DMSO) for 1 h and treated with CA140 (5 μM) or vehicle (1% DMSO) for 23 h (Veh, n = 79; CA140, n = 54; LE300, n = 72; LE300 + CA140, n = 62). **E–H** Immunostaining of p-CaMKIIα or p-ERK in GFP-transfected PHNs treated with CA140 (5 μM) or vehicle (1% DMSO) for 24 h (p-CaMKIIα: Veh, n = 93; CA140, n = 98; p-ERK: Veh, n = 29; CA140, n = 28). **I–L** Immunostaining of p-CaMKIIα or p-ERK in GFP-transfected PHNs treated with LE300 (10 μM) or vehicle (1% DMSO) for 24 h (p-CaMKIIα: Veh, n = 99; LE300, n = 85; p-ERK: Veh, n = 78; LE300, n = 93). Scale bar = 10 μm. **M–P** GFP-transfected PHNs were pretreated with vehicle (1% DMSO), CaMKIIα inhibitor (10 μM), or ERK inhibitor (PD98059) for 1 h and treated with CA140 (5 μM) or vehicle (1% DMSO) for 23 h. Then, dendritic spine number was measured (KN93: Veh, n = 37; CA140, n = 41; KN93 + Veh, n = 36; KN93 + CA140, n = 33; PD98059: Veh, n = 49; CA140, n = 45; PD98059 + Veh, n = 24; PD98059 + CA140, n = 34). Scale bar = 20 μm. *$p < 0.05$, **$p < 0.01$, ***$p < 0.001$

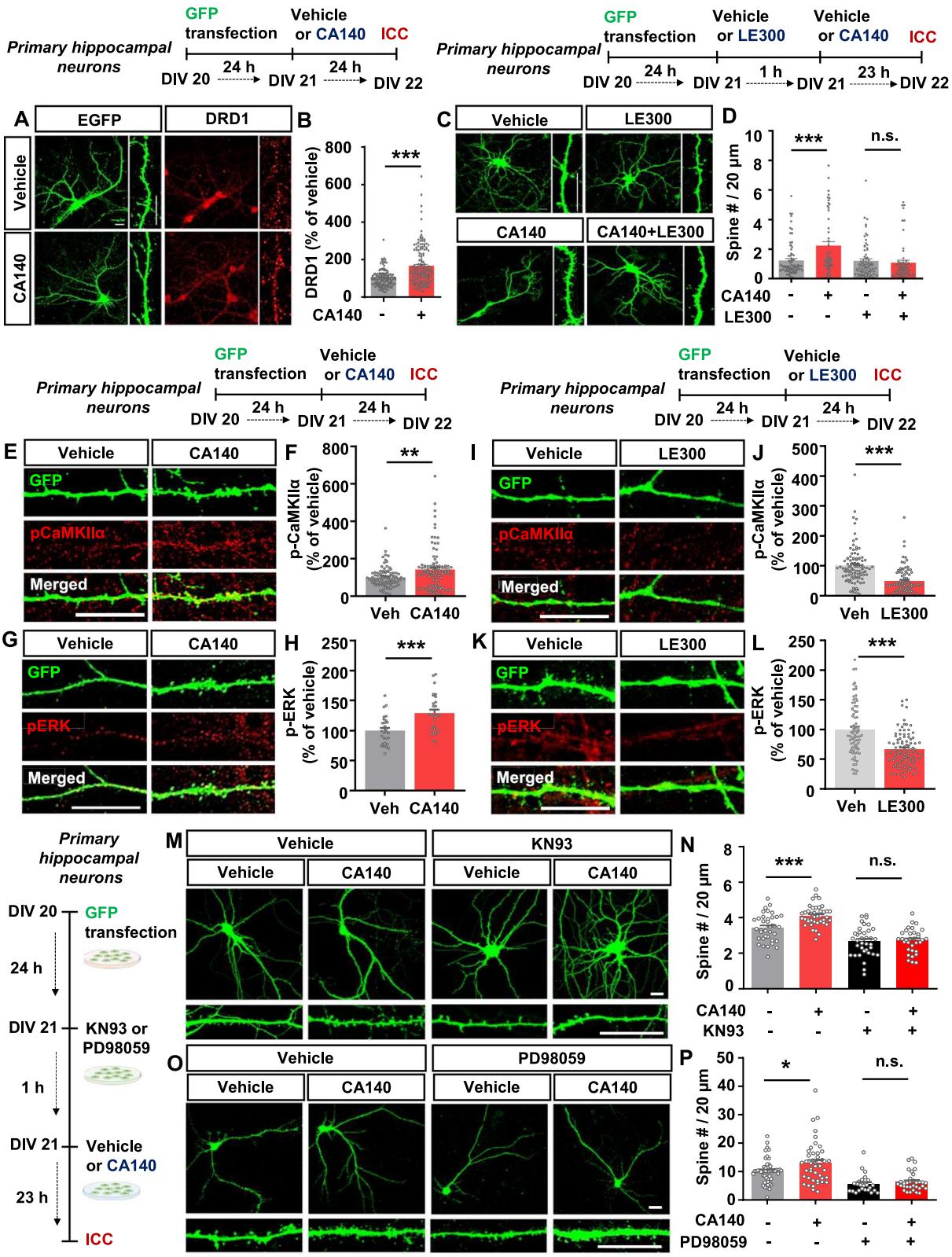

Fig. 11 (See legend on previous page.)

in Aβ aggregation and tauopathy. For example, a DRD1 agonist, A68930 alleviates Aβ-mediated neuropathology, including memory deficits and neuroinflammatory responses, in Aβ-treated WT mice [65]. Moreover, a DRD1 agonist blocks the interaction of Aβ with growth hormone secretagogue receptor 1α (GHSR1α), which is involved in hippocampal plasticity [66]. Overall, these observations indicate that DA and its receptor DRD1 might suppress Aβ pathogenic processes. In the present study, we found that the DA analogue CA140 directly bound aggregated Aβ and inhibited Aβ/Tau fibrillation (Fig. 1). Moreover, we discovered that CA140 reduced Aβ levels in vitro and attenuated Aβ plaque deposition and tau hyperphosphorylation in aged 5xFAD mice (Fig. 1). Based on these results, we hypothesized that the DA analogue CA140 modulates AD pathologies through effects on its receptor DRD1. To test this hypothesis, we examined the effects of CA140 on AD pathologies in an aged AD mouse model. We found that CA140 did not reduce Aβ plaque deposition in 5xFAD mice in which DRD1 was knocked down (Fig. 8). Our results and the literature indicate that CA140 binds directly/indirectly to DRD1 and downregulates AD pathologies under pathological conditions. It is also possible that CA140 directly interacts with Aβ to alter AD pathologies via bidirectional pathways, which we will address in a future study.

Our mRNA-seq analysis identified molecular signatures associated with the actions of CA140 in early-phase AD mice. CA140 treatment altered the mRNA expression of 822 genes involved in various cellular processes, including 40 genes involved in inflammatory response-related cellular processes (Fig. 2, Tables S2 and S3). Among these 40 genes, we focused on the effects of CA140 on neuroinflammation, including NLRP3 inflammasome activation, a key regulator of innate immunity, and IL-1β secretion from microglia [67]. Recent studies have shown that DA administration inhibits NLRP3 inflammasome activation and IL-1β secretion in primary human microglia [16, 68]. In the present study, we investigated the effect of CA140 on reactive gliosis in various stages and models of AD (early/late-phase AD mouse models and PACs and PMCs from 5xFAD mice) at both the mRNA and protein levels. We found that in 3-month-old 5xFAD mice, CA140 treatment significantly downregulated the mRNA levels of reactive gliosis markers, including *trem2/grn* (MGnDs), *clec7a/itgax* (DAMs), *cxcl10* (AD-associated RAs), and *cr3/c1qa* (interactions of RAs and DAMs), and the proinflammatory mediator *nlrp3/il-1β* (Fig. 2). In addition, in 8-month-old 5xFAD mice, CA140 treatment significantly reduced neuroinflammatory dynamics, including the protein expression of markers of AD-associated reactive gliosis (CXCL10), NLRP3/IL-1β, and a marker of interactions of RAs and DAMs (C1QA) (Figs. 3, 4). Furthermore, in PACs or PMCs from 5xFAD mice, CA140 downregulated cell signaling and secreted protein (*s100β, cxcl10*) markers of RAs and markers of PAMs (*gpnmb*), LDAMs (*cln3*), and interactions of RAs and DAMs (*cr3, c1qa*) and upregulated homeostatic microglial markers (*cx3cr1, p2ry12*) (Fig. 5).

Our findings raise the following question: why did CA140 downregulate MGnD and DAM markers in aged 5xFAD mice but not in PMCs from 5xFAD mice? In 5xFAD mice, AD pathology begins to develop at 2–3 months of age, but the primary glial cells were isolated from P1–P2 5xFAD pups, which may not have been old enough to reflect the disease-associated state. PAM populations have been identified in developing microglia (P7 AD mouse pups), and the expression of the C1 cluster of PAM markers (*gpnmb, igf1, spp1, clec7a*) was also upregulated in MGnDs [45]. The present study found that in PMCs from P1–2 5xFAD pups, CA140 treatment downregulated a PAM marker *gpnmb* whose level was increased in MGnD implying that CA140 can mitigate AD-like pathologies even in the developing state. A future study will address whether CA140 modulates the populations of AD-mediated reactive microglia (MGnDs, DAMs, LDAMs) in PMCs from early- and late-phase AD mice.

CA140 treatment also affected the expression of genes in the Toll-like receptor signaling pathway. *TLR2/4* expression is increased on glial cells surrounding Aβ proteins [69–71]. Moreover, TLR4 polymorphisms are protective against AD, and cytokine secretion is reduced in a mouse model of AD in which TLR4 is knocked out, leading to increased glial cell activation in the brain [72–74]. Additional analyses of the genes that are differentially expressed following CA140 treatment will help elucidate their roles in neuroinflammation under normal and pathological conditions.

Scopolamine (SCO) induces cognitive decline by antagonizing muscarinic cholinergic receptors (mAChR) and is widely used in models of cognitive decline (e.g., dementia and amnesia) [75–78]. Interestingly, in the present study, we observed that SCO treatment decreased the number of cortical dendritic spines but not the number of hippocampal AO dendritic spines (Fig. 6). What is the basis of this region-specific antagonistic effect of SCO on dendritic spine formation in the brains of WT mice? Because SCO is a mAChR antagonist, differences in the distribution of mAChR between hippocampal AO/BS and cortical AO/BS may explain this discrepancy in the decrease in dendritic spine number. Specifically, mAChR immunoreactivity is observed in apical dendrites, basal dendrites, and soma of cortical layer V pyramidal cells [79], whereas in the hippocampal CA1 region, mAChR

immunoreactivity is predominantly distributed in basal dendrites and soma of pyramidal cells and is largely absent from naïve apical dendrites [79]. On the basis of previous reports and our findings, we speculate that the antagonistic effect of SCO on dendritic spine formation is enhanced in strongly mAChR-immunoreactive regions (cortical AO/BS and hippocampal BS) compared with weakly mAChR-immunoreactive regions (hippocampal AO). The influence of the differential distribution of mAChR on the effect of SCO on the activation of cholinergic signaling to regulate dendritic spine formation will be investigated in a subsequent study.

SCO reduces DA turnover in the hippocampus and frontal cortex, and stimulation of DA receptors rescues SCO-induced amnesia [80]. Interestingly, a DRD1 agonist improves SCO-induced cognitive decline by increasing the secretion of acetylcholine, an essential neurotransmitter for synaptic plasticity [81]. In line with previous reports, we found that CA140 treatment rescued SCO-mediated memory deficits and dendritic spine loss in WT mice (Fig. 6). These results suggest that CA140 affects DA metabolism and/or acetylcholine secretion to alleviate SCO-induced memory impairment. Strikingly, we found that CA140 treatment completely recovered SCO-induced LTP impairments at hippocampal SC-CA1 synapses (Fig. 6). Given that LTP impairments in the hippocampus can be rescued by activation of cholinergic signaling [82, 83] or DA receptor agonists [84], our findings imply that CA140 might modulate hippocampal LTP by interacting with dopaminergic and/or cholinergic signaling. In a future study, we will examine whether CA140 modulates the cholinergic system to regulate cognitive/synaptic function in SCO-treated WT mice.

DA receptors ($DRD_{1\text{-}5}$) are distributed throughout the hippocampus [9], implicating the DA system in regulating learning and memory and dendritic spine formation [8, 85]. Specifically, DA promotes dendritic spine formation via DRD1 and DRD2 and participates in dendritic spine enlargement and structural plasticity [12]. In addition, experiments in mouse models have shown that manipulating the activities of DRD1 and/or DRD5 affects recognition memory enhancement and hippocampal memory consolidation [13]. Furthermore, dorsal hippocampal DA originating from the locus coeruleus enhances spatial memory via DRD1/5 [58]. Here, we investigated the effects of CA140 on synaptic/cognitive function and its molecular mechanisms of action under pathological conditions and found that CA140 acted as a DRD1 *agonist* to rescue long-term memory/dendritic spine loss and improve synaptophysin expression in aged 5xFAD mice (Figs. 7,8). We next determined whether CA140 regulates synaptic and cognitive function in aged AD mice via Ras-CaMKIIa-ELK1 signaling, which is involved in Aβ-mediated synaptic dysfunction [53, 86]. Phosphorylation of ELK1 initiates neuronal death by enabling the translocation of ELK1 from dendrites to the nucleus and thus is involved in the progression of neurodegenerative diseases (e.g., AD and PD) [87, 88]. Importantly, we demonstrated that treatment with control shRNA and treatment downregulated pELK-1 expression in aged 5xFAD mice, whereas treatment with DRD1 shRNA and CA140 did not significantly decrease pELK-1 expression compared with treatment with DRD1 shRNA and vehicle (Fig. 9). These data indicate that DRD1/ELK-1 might be involved in the positive effects of CA140 on cognitive function in 8-month-old 5xFAD mice. Of course, it is possible that CA140 also directly interacts with Aβ (e.g., via bidirectional pathways involving DRD1 and Aβ) or DRD2 (which is involved in cortical synaptic pruning [89]) to alter synaptic/cognitive function in aged AD mice. Further study will address whether CA140 cooperate with Aβ or DRD2 to regulate AD pathologies and will investigate other possibilities and underlying mechanisms in AD mice model. Interestingly, mRNA-seq analysis revealed that CA140 treatment upregulated the expression of *ngf, tac1*, and *egr1*, which are involved in synaptic function and learning and memory [90–92], in 3-month-old 5xFAD mice (Fig. 2). In animal models and patients with AD, *Tac1* expression is downregulated in the hippocampus, making *tac1* a potential target gene for the treatment of cognitive memory impairments [92]. In animal models of memory deficits, NGF is involved in improving hippocampal/cortical synaptic formation, cholinergic transmission, and spatial memory [91, 93]. *egr1* mRNA and EGR1 protein levels are reduced in the cortex and hippocampus in late-phase AD animal models [90, 94]. It is possible that CA140 improves cognitive and synaptic function by modulating *ngf, tac1*, and *egr1* expression in 5xFAD mice. Further studies will reveal the specific mechanisms by which CA140 enhances synaptic plasticity and memory in mouse models of AD (including young vs. aged AD models).

Under pathological conditions, CA140 treatment alleviated synaptic/cognitive impairments and AD pathologies in partial regulation of DRD1/ELK-1 signaling in aged 5xFAD mice (Fig. 8). We therefore investigated the effects of CA140 on synaptic and cognitive function under normal conditions and whether these effects also involved with DRD1/ELK-1 signaling. We found that CA140 treatment improved cognitive and synaptic function via DRD1 signaling in WT mice (Fig. 9). CA140 treatment did not affect ELK-1 signaling but showed tendency to increase CaMKIIα signaling in WT mice (Fig. 9), suggesting that CA140 improves synaptic and cognitive function through DRD1/CaMKIIα but not ELK-1 under normal conditions. Why does

the DA analogue CA140 differentially regulate downstream signaling under normal and pathological conditions? DRD1 expression is reduced in patients with AD (pathological conditions) compared with healthy controls (normal conditions) [10], which may affect DRD1-mediated downstream signaling under pathological conditions. The reduced expression of DRD1 under pathological conditions may underlie the differential effects of the DRD1–CA140 association under pathological and normal conditions. The specific mechanism by which CA140 differentially modulates DRD1-mediated downstream signaling under normal and pathological conditions will be explored in a future study.

In WT mice, the DA-DRD1 interaction regulates hippocampal synaptic plasticity via Gαq-CaMKIIα signaling [95]. In addition, the RAS/CaMKIIα/ERK pathway is a critical mediator of dendritic spine formation, neuronal plasticity, and cognitive function through regulation of the α-amino-3-hydroxy-5-methyl-4-isoxazolepropionic acid receptor (AMPAR) and N-methyl-D-aspartate receptor (NMDAR) [96–101]. In the present study, we explored the molecular mechanisms by which CA140 affects synaptic function and molecular targeting/signaling under normal conditions in PHNs. We found that CA140 increased CaMKIIα/ERK phosphorylation in PHNs, whereas a DRD1 antagonist (LE300) decreased CaMKIIα/ERK phosphorylation (Fig. 11). Notably, inhibition of CaMKIIα or ERK eliminated the CA140-induced increase in dendritic spine number in PHNs (Fig. 11). Why do the effects of CA140 on downstream CaMKIIα and ERK signaling differ between PHNs and WT mice? Compared with PHNs, whole brain lysates contain multiple types of cells, including microglia, neurons, and astrocytes; these additional cells may influence the effects of CA140 on p-CaMKIIα and p-ERK expression in WT mice. In a future study, we will systematically investigate the effects of CA140 on CaMKIIα/ERK signaling in glial cells (i.e., microglia vs. astrocytes) in vitro and in vivo and compare them with the effects of CA140 on CaMKIIα/ERK signaling in PHNs. Our data suggest that CA140 promotes synaptic function by modulating DRD1/CaMKIIα and/or ERK signaling in PHNs and/or WT mice. Collectively, our findings suggest that CA140 enhances synaptic function and long-term memory by activating DRD1 signaling under normal and pathological conditions. However, it is possible that CA140 affects other synaptic and cognitive function-related signaling networks via bi- and/or multidirectional pathways. Additional studies are needed to unveil the specific mechanisms of action by which CA140 differentially regulates cognitive and synaptic function under pathological and normal conditions.

Conclusions

This study demonstrates that the DA analogue CA140 has novel therapeutic effects on Aβ/tau pathology and synaptic/cognitive function under normal and pathological conditions. In aged 5xFAD mice, CA140 treatment alleviates Aβ accumulation, tau phosphorylation, and deficits in long-term memory, dendritic spine formation, synaptic function and LTP through DRD1. In addition, CA140 ameliorates reactive gliosis in 5xFAD mice, PACs and PMCs. In WT mice and PHNs, CA140 treatment promotes synaptic and cognitive function via DRD1/CaMKIIα and/or ERK signaling. Collectively, these findings suggest that CA140 is a multitarget therapeutic drug for neurodegenerative diseases, including AD.

Abbreviations

AD	Alzheimer's disease
CaMKII	Calcium–calmodulin-dependent protein kinase II
DA	Dopamine
DRD1	Dopamine receptor D1
ERK	Extracellular signal-regulated kinase
LTP	Long-term potentiation
mEPSC	Miniature excitatory postsynaptic current
NLRP3	Nucleotide-binding domain, leucine-rich–containing family, pyrin domain–containing-3
SCO	Scopolamine
TLR	Toll-like receptor
PHN	Primary hippocampal neuron

Supplementary Information

The online version contains supplementary material available at https://doi.org/10.1186/s12974-024-03180-x.

Supplementary file 1.

Supplementary file 2.

Supplementary file 3.

Acknowledgements

Confocal microscopy (Nikon, T-RCP) data were acquired at the Advanced Neural Imaging Center at the Korea Brain Research Institute (KBRI). We thank previous and current neurodegenerative diseases lab members, specifically Dr. Jin Han Nam, Dr. Youngpyo Nam, Dr. Hee-Jeong Choi, HyunHee Park for editing, technical assistance/support for in vitro and in vivo work, valuable comments, and behavior studies in our manuscript. In addition, we thank Dr. Daniel Pak, Dr. Jeongyeon Kim. and Dr. Misun Kang's technical assistance/support for in vitro and in vivo work.

Author contributions

J.Y., J. I. K., and H.S.H. conceived and participated in the design of the study. S.C., H.J.L., H.E.L., J.Y., Y. L., M.D.S., Y.H.L., J.I.K., and H.S.H. wrote the manuscript. S.C. analyzed the RNA sequencing data. H.J.L., J.K., Y. J., Y.L., S.Y.S., H.P., G.L., R.S.E, S.C.L. performed in vitro and vivo experiments, quantification of data, and histological analysis. H.E.L conducted LTP experiments. H.J.L., H.E.L., and H.Y.K performed the experiments, quantification of data, and statistical analysis during the revision. All authors read and approved the final manuscript.

Funding

This work was supported by the Basic Science Research Program through the National Research Foundation of Korea (NRF) funded by the Ministry of Science and ICT (Grants 2019R1A2B5B01070108 to H.S.H. and 2021R1A4A1031644, 2021M3A9G8022960, 2022M325E8017907, and 2023R1A2C1006489 to J.I.K, RS-2023-00253215 to S.C.) and the KBRI basic research program through KBRI funded by the Ministry of Science, ICT, and

Future Planning (Grants 24-BR-02-03, 23-BR-02-12, 24-BR-03-07, 24-BR-05-02, 24-BR-03-01, and 24-BR-03-05 to H.S.H., 21-BR-02-12 to J.I.K., and 23-BR-01-02 to S.C.). This work was also supported by the National Institute on Aging at the National Institutes of Health (award number R01AG053577 to G.L., R.S.E, S.C.L. and J.Y.). In addition, this work was supported by a National Research Foundation of Korea (NRF) grant funded by the Korean government (Grant NRF-2022R1A2C1011793 to Y.-H.L.), the KBSI fund (grant A439200 to Y.-H.L.) and the Korea Ministry of Science and ICT's Special Account for Regional Balanced Development for Commercialization supervised by the NIPA (National IT Industry Promotion Agency) to support AI-based digital medical devices for neurodevelopmental disorders (H0301-24-1001 to H.S.H.).

Availability of data and materials
All data generated and/or analyzed during this study are included in this article and the supplementary information files.

Declarations

Ethical approval and consent to participate
All in vivo experiments were performed in accordance with approved animal protocols and guidelines established by the Korea Brain Research Institute (IACUC-2016–0013, IACUC-2018-0018).

Consent for publication
Not applicable.

Competing interests
The authors declare no competing interests.

Author details
[1]Neurovascular Unit, Korea Brain Research Institute (KBRI), 61, Cheomdan-ro, Dong-gu, Daegu 41068, Republic of Korea. [2]Neurodegenerative Unit, Korea Brain Research Institute (KBRI), 61, Cheomdan-ro, Dong-gu, Daegu 41068, Republic of Korea. [3]Department of Biological Sciences, Ulsan National Institute of Science and Technology (UNIST), 50 UNIST-Gil, Ulsan 44919, Republic of Korea. [4]Biopharmaceutical Research Center, Korea Basic Science Institute (KBSI), Ochang, ChungBuk 28119, Republic of Korea. [5]Department of Chemistry and Biochemistry, University of California, San Diego, La Jolla, CA 92093-0358, USA. [6]College of Pharmacy and Department of Molecular Science and Technology, Ajou University, Suwon, Gyeonggi 16499, Republic of Korea. [7]Department of Brain & Cognitive Sciences, Daegu Gyeongbuk Institute of Science & Technology (DGIST), Daegu 42988, Republic of Korea. [8]Bio-Analytical Science, University of Science and Technology (UST), Daejeon 34113, Republic of Korea. [9] Department of Systems Biotechnology, Chung-Ang University, Gyeonggi 17546, Republic of Korea. [10]Department of Neural Development and Disease, Korea Brain Research Institute (KBRI), 61 Cheomdan-ro, Dong-gu, Daegu 41068, Republic of Korea.

Received: 10 July 2023 Accepted: 17 July 2024
Published online: 11 August 2024

References

1. DeTure MA, Dickson DW. The neuropathological diagnosis of Alzheimer's disease. Mol Neurodegener. 2019;14(1):32.
2. DeKosky ST, Scheff SW. Synapse loss in frontal cortex biopsies in Alzheimer's disease: correlation with cognitive severity. Ann Neurol. 1990;27(5):457–64.
3. Sobue A, Komine O, Yamanaka K. Neuroinflammation in Alzheimer's disease: microglial signature and their relevance to disease. Inflamm Regen. 2023;43(1):26.
4. Muzio L, Viotti A, Martino G. Microglia in neuroinflammation and neurodegeneration: from understanding to therapy. Front Neurosci. 2021;15:742065.
5. Perez-Nievas BG, Serrano-Pozo A. Deciphering the astrocyte reaction in Alzheimer's disease. Front Aging Neurosci. 2018;10:114.
6. Selkoe DJ. Resolving controversies on the path to Alzheimer's therapeutics. Nat Med. 2011;17(9):1060–5.
7. Kramar CP, Chefer VI, Wise RA, Medina JH, Barbano MF. Dopamine in the dorsal hippocampus impairs the late consolidation of cocaine-associated memory. Neuropsychopharmacology. 2014;39(7):1645–53.
8. Yagishita S, Hayashi-Takagi A, Ellis-Davies GC, Urakubo H, Ishii S, Kasai H. A critical time window for dopamine actions on the structural plasticity of dendritic spines. Science. 2014;345(6204):1616–20.
9. Rezaei M, Sadeghian A, Roohi N, Shojaei A, Mirnajafi-Zadeh J. Epilepsy and dopaminergic system. Physiol Pharmacol. 2017;21(1):1–14.
10. Pan X, Kaminga AC, Wen SW, Wu X, Acheampong K, Liu A. Dopamine and dopamine receptors in Alzheimer's disease: a systematic review and network meta-analysis. Front Aging Neurosci. 2019;11:175.
11. Dubovyk V, Manahan-Vaughan D. Gradient of expression of dopamine D2 receptors along the dorso-ventral axis of the hippocampus. Front Synaptic Neurosci. 2019;11:28.
12. Fasano C, Bourque MJ, Lapointe G, Leo D, Thibault D, Haber M, Kortleven C, Desgroseillers L, Murai KK, Trudeau LE. Dopamine facilitates dendritic spine formation by cultured striatal medium spiny neurons through both D1 and D2 dopamine receptors. Neuropharmacology. 2013;67:432–43.
13. de Lima MN, Presti-Torres J, Dornelles A, Scalco FS, Roesler R, Garcia VA, Schroder N. Modulatory influence of dopamine receptors on consolidation of object recognition memory. Neurobiol Learn Mem. 2011;95(3):305–10.
14. Lemon N, Manahan-Vaughan D. Dopamine D1/D5 receptors gate the acquisition of novel information through hippocampal long-term potentiation and long-term depression. J Neurosci. 2006;26(29):7723–9.
15. Xia QP, Cheng ZY, He L. The modulatory role of dopamine receptors in brain neuroinflammation. Int Immunopharmacol. 2019;76: 105908.
16. Pike AF, Longhena F, Faustini G, van Eik JM, Gombert I, Herrebout MAC, Fayed M, Sandre M, Varanita T, Teunissen CE, et al. Dopamine signaling modulates microglial NLRP3 inflammasome activation: implications for Parkinson's disease. J Neuroinflamm. 2022;19(1):50.
17. Lee JY, Nam JH, Nam Y, Nam HY, Yoon G, Ko E, Kim SB, Bautista MR, Capule CC, Koyanagi T, et al. The small molecule CA140 inhibits the neuroinflammatory response in wild-type mice and a mouse model of AD. J Neuroinflamm. 2018;15(1):286.
18. Na D, Zhang J, Beaulac HJ, Piekna-Przybylska D, Nicklas PR, Kiernan AE, White PM. Increased central auditory gain in 5xFAD Alzheimer's disease mice as an early biomarker candidate for Alzheimer's disease diagnosis. Front Neurosci. 2023;17:1106570.
19. Abaandou L, Quan D, Shiloach J. Affecting HEK293 cell growth and production performance by modifying the expression of specific genes. Cells. 2021;10(7):1667.
20. Hoe HS, Freeman J, Rebeck GW. Apolipoprotein E decreases tau kinases and phospho-tau levels in primary neurons. Mol Neurodegener. 2006;1:18.
21. Pak DT, Yang S, Rudolph-Correia S, Kim E, Sheng M. Regulation of dendritic spine morphology by SPAR, a PSD-95-associated RapGAP. Neuron. 2001;31(2):289–303.
22. van Gijsel-Bonnello M, Baranger K, Benech P, Rivera S, Khrestchatisky M, de Reggi M, Gharib B. Metabolic changes and inflammation in cultured astrocytes from the 5xFAD mouse model of Alzheimer's disease: alleviation by pantethine. PLoS ONE. 2017;12(4): e0175369.
23. Ryu KY, Lee HJ, Woo H, Kang RJ, Han KM, Park H, Lee SM, Lee JY, Jeong YJ, Nam HW, et al. Dasatinib regulates LPS-induced microglial and astrocytic neuroinflammatory responses by inhibiting AKT/STAT3 signaling. J Neuroinflamm. 2019;16(1):190.
24. Ehrlich RS, Shiao AL, Li M, Teppang KL, Jeoung KY, Theodorakis EA, Yang J. Exploring the effect of aliphatic substituents on aryl cyano amides on enhancement of fluorescence upon binding to amyloid-beta aggregates. ACS Chem Neurosci. 2021;12(15):2946–52.
25. Capule CC, Brown C, Olsen JS, Dewhurst S, Yang J. Oligovalent amyloid-binding agents reduce SEVI-mediated enhancement of HIV-1 infection. J Am Chem Soc. 2012;134(2):905–8.
26. Roche J, Shen Y, Lee JH, Ying J, Bax A. Monomeric Abeta(1–40) and Abeta(1–42) peptides in solution adopt very similar ramachandran map distributions that closely resemble random coil. Biochemistry. 2016;55(5):762–75.
27. Nam Y, Joo B, Lee JY, Han KM, Ryu KY, Koh YH, Kim J, Koo JW, We YM, Hoe HS. ALWPs improve cognitive function and regulate Abeta

plaque and tau hyperphosphorylation in a mouse model of Alzheimer's disease. Front Mol Neurosci. 2019;12:192.
28. Lee HJ, Hoe HS. Inhibition of CDK4/6 regulates AD pathology, neuroinflammation and cognitive function through DYRK1A/STAT3 signaling. Pharmacol Res. 2023;190: 106725.
29. Lee HJ, Jeon SG, Kim J, Kang RJ, Kim SM, Han KM, Park H, Kim KT, Sung YM, Nam HY, et al. Ibrutinib modulates Abeta/tau pathology, neuroinflammation, and cognitive function in mouse models of Alzheimer's disease. Aging Cell. 2021;20(3): e13332.
30. Trapnell C, Pachter L, Salzberg SL. TopHat: discovering splice junctions with RNA-Seq. Bioinformatics. 2009;25(9):1105–11.
31. Anders S, Pyl PT, Huber W. HTSeq–a Python framework to work with high-throughput sequencing data. Bioinformatics. 2015;31(2):166–9.
32. Robinson MD, Oshlack A. A scaling normalization method for differential expression analysis of RNA-seq data. Genome Biol. 2010;11(3):R25.
33. Love MI, Huber W, Anders S. Moderated estimation of fold change and dispersion for RNA-seq data with DESeq2. Genome Biol. 2014;15(12):550.
34. Sherman BT, Hao M, Qiu J, Jiao X, Baseler MW, Lane HC, Imamichi T, Chang W. DAVID: a web server for functional enrichment analysis and functional annotation of gene lists (2021 update). Nucleic Acids Res. 2022;50(W1):W216–21.
35. Kanehisa M, Furumichi M, Sato Y, Ishiguro-Watanabe M, Tanabe M. KEGG: integrating viruses and cellular organisms. Nucleic Acids Res. 2021;49(D1):D545–51.
36. Martens M, Ammar A, Riutta A, Waagmeester A, Slenter DN, Hanspers K, Miller RA, Digles D, Lopes EN, Ehrhart F, et al. WikiPathways: connecting communities. Nucleic Acids Res. 2021;49(D1):D613–21.
37. Cataldi R, Chia S, Pisani K, Ruggeri FS, Xu CK, Sneideris T, Perni M, Sarwat S, Joshi P, Kumita JR, et al. A dopamine metabolite stabilizes neurotoxic amyloid-beta oligomers. Commun Biol. 2021;4(1):19.
38. Kinney JW, Bemiller SM, Murtishaw AS, Leisgang AM, Salazar AM, Lamb BT. Inflammation as a central mechanism in Alzheimer's disease. Alzheimers Dement. 2018;4:575–90.
39. Bernaus A, Blanco S, Sevilla A. Glia crosstalk in neuroinflammatory diseases. Front Cell Neurosci. 2020;14:209.
40. Lin W, Li Z, Liang G, Zhou R, Zheng X, Tao R, Huo Q, Su C, Li M, Xu N, et al. TNEA therapy promotes the autophagic degradation of NLRP3 inflammasome in a transgenic mouse model of Alzheimer's disease via TFEB/TFE3 activation. J Neuroinflamm. 2023;20(1):21.
41. Escartin C, Galea E, Lakatos A, O'Callaghan JP, Petzold GC, Serrano-Pozo A, Steinhauser C, Volterra A, Carmignoto G, Agarwal A, et al. Reactive astrocyte nomenclature, definitions, and future directions. Nat Neurosci. 2021;24(3):312–25.
42. Yu W, Li Y, Zhong F, Deng Z, Wu J, Yu W, Lu Y. Disease-associated neurotoxic astrocyte markers in Alzheimer disease based on integrative single-nucleus RNA sequencing. Cell Mol Neurobiol. 2024;44(1):20.
43. Jo KW, Lee D, Cha DG, Oh E, Choi YH, Kim S, Park ES, Kim JK, Kim KT. Gossypetin ameliorates 5xFAD spatial learning and memory through enhanced phagocytosis against Abeta. Alzheimers Res Ther. 2022;14(1):158.
44. Paolicelli RC, Sierra A, Stevens B, Tremblay ME, Aguzzi A, Ajami B, Amit I, Audinat E, Bechmann I, Bennett M, et al. Microglia states and nomenclature: a field at its crossroads. Neuron. 2022;110(21):3458–83.
45. Li Q, Cheng Z, Zhou L, Darmanis S, Neff NF, Okamoto J, Gulati G, Bennett ML, Sun LO, Clarke LE, et al. Developmental heterogeneity of microglia and brain myeloid cells revealed by deep single-cell RNA sequencing. Neuron. 2019;101(2):207–23.
46. Lee JS, Kim HG, Lee HW, Han JM, Lee SK, Kim DW, Saravanakumar A, Son CG. Hippocampal memory enhancing activity of pine needle extract against scopolamine-induced amnesia in a mouse model. Sci Rep. 2015;5:9651.
47. Lee HJ, Woo H, Lee HE, Jeon H, Ryu KY, Nam JH, Jeon SG, Park H, Lee JS, Han KM, et al. The novel DYRK1A inhibitor KVN93 regulates cognitive function, amyloid-beta pathology, and neuroinflammation. Free Radic Biol Med. 2020;160:575–95.
48. Dorostkar MM, Zou C, Blazquez-Llorca L, Herms J. Analyzing dendritic spine pathology in Alzheimer's disease: problems and opportunities. Acta Neuropathol. 2015;130(1):1–19.
49. Zhang M, Zhong L, Han X, Xiong G, Xu D, Zhang S, Cheng H, Chiu K, Xu Y. Brain and retinal abnormalities in the 5xFAD mouse model of Alzheimer's disease at early stages. Front Neurosci. 2021;15: 681831.
50. Forner S, Kawauchi S, Balderrama-Gutierrez G, Kramar EA, Matheos DP, Phan J, Javonillo DI, Tran KM, Hingco E, da Cunha C, et al. Systematic phenotyping and characterization of the 5xFAD mouse model of Alzheimer's disease. Sci Data. 2021;8(1):270.
51. Jourdain P, Fukunaga K, Muller D. Calcium/calmodulin-dependent protein kinase II contributes to activity-dependent filopodia growth and spine formation. J Neurosci. 2003;23(33):10645–9.
52. Ohta KI, Suzuki S, Warita K, Kaji T, Kusaka T, Miki T. Prolonged maternal separation attenuates BDNF-ERK signaling correlated with spine formation in the hippocampus during early brain development. J Neurochem. 2017;141(2):179–94.
53. Szatmari EM, Oliveira AF, Sumner EJ, Yasuda R. Centaurin-alpha1-Ras-Elk-1 signaling at mitochondria mediates beta-amyloid-induced synaptic dysfunction. J Neurosci. 2013;33(12):5367–74.
54. Jones MR, Urits I, Wolf J, Corrigan D, Colburn L, Peterson E, Williamson A, Viswanath O. Drug-induced peripheral neuropathy: a narrative review. Curr Clin Pharmacol. 2020;15(1):38–48.
55. Arendt T, Gartner U, Seeger G, Barmashenko G, Palm K, Mittmann T, Yan L, Hummeke M, Behrbohm J, Bruckner MK, et al. Neuronal activation of Ras regulates synaptic connectivity. Eur J Neurosci. 2004;19(11):2953–66.
56. Zhu JJ, Qin Y, Zhao M, Van Aelst L, Malinow R. Ras and Rap control AMPA receptor trafficking during synaptic plasticity. Cell. 2002;110(4):443–55.
57. Wu L, D'Amico A, Hochrein H, O'Keeffe M, Shortman K, Lucas K. Development of thymic and splenic dendritic cell populations from different hemopoietic precursors. Blood. 2001;98(12):3376–82.
58. Kempadoo KA, Mosharov EV, Choi SJ, Sulzer D, Kandel ER. Dopamine release from the locus coeruleus to the dorsal hippocampus promotes spatial learning and memory. Proc Natl Acad Sci USA. 2016;113(51):14835–40.
59. Calabresi P, Picconi B, Tozzi A, Di Filippo M. Dopamine-mediated regulation of corticostriatal synaptic plasticity. Trends Neurosci. 2007;30(5):211–9.
60. Denenberg VH, Kim DS, Palmiter RD. The role of dopamine in learning, memory, and performance of a water escape task. Behav Brain Res. 2004;148(1–2):73–8.
61. Jay TM. Dopamine: a potential substrate for synaptic plasticity and memory mechanisms. Prog Neurobiol. 2003;69(6):375–90.
62. Takeuchi T, Duszkiewicz AJ, Sonneborn A, Spooner PA, Yamasaki M, Watanabe M, Smith CC, Fernandez G, Deisseroth K, Greene RW, et al. Locus coeruleus and dopaminergic consolidation of everyday memory. Nature. 2016;537(7620):357–62.
63. Nam E, Derrick JS, Lee S, Kang J, Han J, Lee SJC, Chung SW, Lim MH. regulatory activities of dopamine and its derivatives toward metal-free and metal-induced amyloid-beta aggregation, oxidative stress, and inflammation in Alzheimer's disease. ACS Chem Neurosci. 2018;9(11):2655–66.
64. Li J, Zhu M, Manning-Bog AB, Di Monte DA, Fink AL. Dopamine and L-dopa disaggregate amyloid fibrils: implications for Parkinson's and Alzheimer's disease. FASEB J. 2004;18(9):962–4.
65. Cheng ZY, Xia QP, Hu YH, Wang C, He L. Dopamine D1 receptor agonist A-68930 ameliorates Abeta(1–42)-induced cognitive impairment and neuroinflammation in mice. Int Immunopharmacol. 2020;88: 106963.
66. Tian J, Guo L, Sui S, Driskill C, Phensy A, Wang Q, Gauba E, Zigman JM, Swerdlow RH, Kroener S, et al. Disrupted hippocampal growth hormone secretagogue receptor 1alpha interaction with dopamine receptor D1 plays a role in Alzheimer's disease. Sci Transl Med. 2019. https://doi.org/10.1126/scitranslmed.aav6278.
67. Latz E, Xiao TS, Stutz A. Activation and regulation of the inflammasomes. Nat Rev Immunol. 2013;13(6):397–411.
68. Yan Y, Jiang W, Liu L, Wang X, Ding C, Tian Z, Zhou R. Dopamine controls systemic inflammation through inhibition of NLRP3 inflammasome. Cell. 2015;160(1–2):62–73.
69. Letiembre M, Liu Y, Walter S, Hao W, Pfander T, Wrede A, Schulz-Schaeffer W, Fassbender K. Screening of innate immune receptors in neurodegenerative diseases: a similar pattern. Neurobiol Aging. 2009;30(5):759–68.

70. Frank S, Copanaki E, Burbach GJ, Muller UC, Deller T. Differential regulation of toll-like receptor mRNAs in amyloid plaque-associated brain tissue of aged APP23 transgenic mice. Neurosci Lett. 2009;453(1):41–4.
71. Walter S, Letiembre M, Liu Y, Heine H, Penke B, Hao W, Bode B, Manietta N, Walter J, Schulz-Schuffer W, et al. Role of the toll-like receptor 4 in neuroinflammation in Alzheimer's disease. Cell Physiol Biochem. 2007;20(6):947–56.
72. Minoretti P, Gazzaruso C, Vito CD, Emanuele E, Bianchi M, Coen E, Reino M, Geroldi D. Effect of the functional toll-like receptor 4 Asp299Gly polymorphism on susceptibility to late-onset Alzheimer's disease. Neurosci Lett. 2006;391(3):147–9.
73. Jin JJ, Kim HD, Maxwell JA, Li L, Fukuchi K. Toll-like receptor 4-dependent upregulation of cytokines in a transgenic mouse model of Alzheimer's disease. J Neuroinflamm. 2008;5:23.
74. Tahara K, Kim HD, Jin JJ, Maxwell JA, Li L, Fukuchi K. Role of toll-like receptor signalling in Abeta uptake and clearance. Brain. 2006;129(Pt 11):3006–19.
75. Preston GC, Brazell C, Ward C, Broks P, Traub M, Stahl SM. The scopolamine model of dementia: determination of central cholinomimetic effects of physostigmine on cognition and biochemical markers in man. J Psychopharmacol. 1988;2(2):67–79.
76. Stone WS, Croul CE, Gold PE. Attenuation of scopolamine-induced amnesia in mice. Psychopharmacology. 1988;96(3):417–20.
77. Ebert U, Kirch W. Scopolamine model of dementia: electroencephalogram findings and cognitive performance. Eur J Clin Invest. 1998;28(11):944–9.
78. Bajo R, Pusil S, Lopez ME, Canuet L, Pereda E, Osipova D, Maestu F, Pekkonen E. Scopolamine effects on functional brain connectivity: a pharmacological model of Alzheimer's disease. Sci Rep. 2015;5:9748.
79. van der Zee EA, Luiten PG. Muscarinic acetylcholine receptors in the hippocampus, neocortex and amygdala: a review of immunocytochemical localization in relation to learning and memory. Prog Neurobiol. 1999;58(5):409–71.
80. Memo M, Missale C, Trivelli L, Spano PF. Acute scopolamine treatment decreases dopamine metabolism in rat hippocampus and frontal cortex. Eur J Pharmacol. 1988;149(3):367–70.
81. Piri M, Rostampour M, Nasehi M, Zarrindast MR. Blockade of the dorsal hippocampal dopamine D1 receptors inhibits the scopolamine-induced state-dependent learning in rats. Neuroscience. 2013;252:460–7.
82. Drever BD, Riedel G, Platt B. The cholinergic system and hippocampal plasticity. Behav Brain Res. 2011;221(2):505–14.
83. Chen J, Nakamura M, Kawamura T, Takahashi T, Nakahara D. Roles of pedunculopontine tegmental cholinergic receptors in brain stimulation reward in the rat. Psychopharmacology. 2006;184(3–4):514–22.
84. Yuan Xiang P, Janc O, Grochowska KM, Kreutz MR, Reymann KG. Dopamine agonists rescue Abeta-induced LTP impairment by Src-family tyrosine kinases. Neurobiol Aging. 2016;40:98–102.
85. Kramar CP, Barbano MF, Medina JH. Dopamine D1/D5 receptors in the dorsal hippocampus are required for the acquisition and expression of a single trial cocaine-associated memory. Neurobiol Learn Mem. 2014;116:172–80.
86. Tong L, Balazs R, Thornton PL, Cotman CW. Beta-amyloid peptide at sublethal concentrations downregulates brain-derived neurotrophic factor functions in cultured cortical neurons. J Neurosci. 2004;24(30):6799–809.
87. Sharma A, Callahan LM, Sul JY, Kim TK, Barrett L, Kim M, Powers JM, Federoff H, Eberwine J. A neurotoxic phosphoform of Elk-1 associates with inclusions from multiple neurodegenerative diseases. PLoS ONE. 2010;5(2): e9002.
88. Barrett LE, Sul JY, Takano H, Van Bockstaele EJ, Haydon PG, Eberwine JH. Region-directed phototransfection reveals the functional significance of a dendritically synthesized transcription factor. Nat Methods. 2006;3(6):455–60.
89. Zhang YQ, Lin WP, Huang LP, Zhao B, Zhang CC, Yin DM. Dopamine D2 receptor regulates cortical synaptic pruning in rodents. Nat Commun. 2021;12(1):6444.
90. Hu YT, Chen XL, Huang SH, Zhu QB, Yu SY, Shen Y, Sluiter A, Verhaagen J, Zhao J, Swaab D, et al. Early growth response-1 regulates acetylcholinesterase and its relation with the course of Alzheimer's disease. Brain Pathol. 2019;29(4):502–12.
91. Eu WZ, Chen YJ, Chen WT, Wu KY, Tsai CY, Cheng SJ, Carter RN, Huang GJ. The effect of nerve growth factor on supporting spatial memory depends upon hippocampal cholinergic innervation. Transl Psychiatry. 2021;11(1):162.
92. Liu YJ, Liu TT, Jiang LH, Liu Q, Ma ZL, Xia TJ, Gu XP. Identification of hub genes associated with cognition in the hippocampus of Alzheimer's Disease. Bioengineered. 2021;12(2):9598–609.
93. Garofalo L, Ribeiro-da-Silva A, Cuello AC. Nerve growth factor-induced synaptogenesis and hypertrophy of cortical cholinergic terminals. Proc Natl Acad Sci USA. 1992;89(7):2639–43.
94. Koldamova R, Schug J, Lefterova M, Cronican AA, Fitz NF, Davenport FA, Carter A, Castranio EL, Lefterov I. Genome-wide approaches reveal EGR1-controlled regulatory networks associated with neurodegeneration. Neurobiol Dis. 2014;63:107–14.
95. Kern A, Mavrikaki M, Ullrich C, Albarran-Zeckler R, Brantley AF, Smith RG. Hippocampal dopamine/DRD1 signaling dependent on the ghrelin receptor. Cell. 2015;163(5):1176–90.
96. Barcomb K, Buard I, Coultrap SJ, Kulbe JR, O'Leary H, Benke TA, Bayer KU. Autonomous CaMKII requires further stimulation by Ca2+/calmodulin for enhancing synaptic strength. FASEB J. 2014;28(8):3810–9.
97. Pi HJ, Otmakhov N, El Gaamouch F, Lemelin D, De Koninck P, Lisman J. CaMKII control of spine size and synaptic strength: role of phosphorylation states and nonenzymatic action. Proc Natl Acad Sci USA. 2010;107(32):14437–42.
98. Ryu HH, Lee YS. Cell type-specific roles of RAS-MAPK signaling in learning and memory: implications in neurodevelopmental disorders. Neurobiol Learn Mem. 2016;135:13–21.
99. Cornelia Koeberle S, Tanaka S, Kuriu T, Iwasaki H, Koeberle A, Schulz A, Helbing DL, Yamagata Y, Morrison H, Okabe S. Developmental stage-dependent regulation of spine formation by calcium-calmodulin-dependent protein kinase IIalpha and Rap1. Sci Rep. 2017;7(1):13409.
100. Wayman GA, Lee YS, Tokumitsu H, Silva AJ, Soderling TR. Calmodulin-kinases: modulators of neuronal development and plasticity. Neuron. 2008;59(6):914–31.
101. Lee YS, Silva AJ. The molecular and cellular biology of enhanced cognition. Nat Rev Neurosci. 2009;10(2):126–40.

Publisher's Note